2mlp

NASA TECHNICAL TRANSLATION NASA TT F 15,707

EXPERIMENTAL INVESTIGATION OF THE FLOW FIELD OF A HOT TURBULENT JET WITH LATERAL FLOW

PART I

L. Harms

Translation of: "Experimentelle Untersuchungen ueber das Stroemungsfeld eines heissen, turbulenten Strahles bei Queranstroemung,"
1. Teilbericht, Deutsche Forschungs- und Versuchsanstalt fuer Luft- und Raumfahrt E. V., Braunschweig, West Germany, Report 1B 157 73 A 18, September 17, 1973, 62 pp.

NATIONAL AERONAUTICS AND SPACE ADMINISTRATION
WASHINGTON, D. C. 20546 JUNE 1974

STANDARD TITLE PAGE

1. Report No. NASA TT F 15,707	2. Government Accession No.	3. Recipient's Catalog No.
4. Title and Subtitle EXPERIMENTAL INVESTIGATION OF THE FLOW FIELD OF A HOT TURBULENT JET WITH LATERAL FLOW		5. Report Date June 17, 1974 6. Performing Organization Code
7. Author(s) L. Harms		8. Performing Organization Report No. 10. Work Unit No. 11. Contract or Grant No. NASw-2483
9. Performing Organization Name and Address SCITRAN Box 5456 Santa Barbara, CA 93108		13. Type of Report and Period Covered Translation
12. Sponsoring Agency Name and Address National Aeronautics and Space Administration Washington, D.C. 20546		14. Sponsoring Agency Code

15. Supplementary Notes

Translation of: "Experimentelle Untersuchungen ueber das Stroemungsfeld eines heissen, turbulenten Strahles bei Queranstroemung," 1. Teilbericht, Deutsche Forschungs- und Versuchs-Anstalt fuer Luft und Raumfahrt E.V., Braunschweig, West Germany, Report IB 157 73 A 18, September 17, 1973, 62 pp.

16. Abstract

In the 3 m wind tunnel of the DFVLR-AVA Goettingen, we measured the three-dimensional flow field of a hot round jet with the effect of a transverse flow using a nine-hole probe at several intersection planes. We investigated the influence of various velocity and temperature conditions on the flow field. The measurements were compared with the results for the cold jet in a transverse flow and this has led to new laws regarding the mixing of a hot jet with its surroundings.

17. Key Words (Selected by Author(s))	18. Distribution Statement
	Unclassified - Unlimited

19. Security Classif. (of this report)	20. Security Classif. (of this page)	21. No. of Pages	22. Price
Unclassified	Unclassified	58	

PRECEDING PAGE BLANK NOT FILMED

TABLE OF CONTENTS

EXPERIMENTAL INVESTIGATION OF THE FLOW FIELD OF A HOT TURBULENT JET WITH LATERNAL FLOW

L. Harms

NOTATION /3*

Geometric Variables (Figure 1)

D	Nozzle exit diameter
F_V	Valve cross section
F_D	Nozzle exhaust cross section
$X, Y, Z \triangleq x, y, z$	Cartesian coordinates (Figure 1)
ϑ	Inclination of the jet with respect to the channel axis ($\vartheta = 90^\circ$ for perpendicular incident flow)

Flow Variables

a	Speed of sound
g	Local total pressure
$\dot{m}$	Mass flux
p	Local static pressure
p_a	Pressure at the outer side of probe
p_o	Pressure on top side of probe
p_s	Pressure on shaft side of probe
p_t	Ambient pressure
p_u	Pressure along lower side of probe
q	Local stagnation pressure
V	Magnitude of local velocity
V_∞	Incident flow velocity

*Numbers in margin indicate pagination of original foreign text.

V_j	Jet velocity at nozzle exit point
V_x, V_y, V_z	x component of local velocity in x, y, and z directions, respectively.
α_w	Angle between local flow direction /4 and horizontal channel central plane (downwind angle)
β_w	Angle between the local flow direction and the x-z plane (side wind angle)
Re_D	Reynolds number $Re = V_\infty \cdot D/\nu$; ν = kinematic viscosity
Ma_D	Mach number $Ma = V_j/a_j$

Other variables and abbreviations

t	Temperature in ° Celsius
T	Absolute temperature
$\theta = T_j/T_\infty$	Temperature ratio of nozzle jet and surroundings
$\psi = V_j/V_\infty$	Ratio of velocity of nozzle jet and incident flow
$\phi = (\rho_j V_j^2)/(\rho_\infty V_\infty^2)$	Ratio of momentum flows of nozzle jet and incident flow (momentum ratio)
$\varphi = \alpha_w/\vartheta$	Ratio of local flow direction α_w and nozzle inclination angle ϑ
$\Delta P_\beta = p_a - p_s$	Pressure difference because of side wind
$\Delta P_\alpha = p_0 - p_u$	Pressure difference because of downwind

Subscripts

m	Uncorrected measured value
j	Value referred to jet at nozzle exit point
x, y, z	Values in the direction of the coordinate axes x, y, and z
∞	Undisturbed flow
M	Value in the jet center
H	Value in the electrical heater
R	Value ahead of nozzle exit point
1, 2, 3, ...	Measurement point index

I. INTRODUCTION

The mixing process between two intersecting flows represents /5 one of the most elementary processes in fluid mechanics. Often a configuration occurs in which one flow has a much lower mass flux than the other.

Examples of such flows can be found in environmental science, where the distribution of smoke plumes of chimneys in the atmosphere [1] or the mixing of warm cooling water flows in rivers [2] have become very important.

In aviation technology, we are interested in the variation and propagation region of the jet in connection with the development of short takeoff or vertical takeoff aircraft [3]. For the case of jet supported flight, we have large influences of the jet on the lift and the drag [4] during the takeoff and landing phases. Investigations of jets in transverse flows are also important in connection with the expulsion of cooling agents into the boundary layer of space vehicles during hypersonic flight [5].

Another application of mixing processes in jets in transverse flows occurs in the cooling of walls in the vicinity of hot combustion gases in gas turbines [6]. In the gas turbine combustion chambers, a cooling of the flow near the wall is brought about by expelling cold air through the holes in the wall. Even though several jets are used for effective cooling, it is appropriate to study the basic flow processes using a single jet.

The first theoretical treatment of a jet in a transverse wind was investigated rather early in the region near the point where the jet emerges. The VTOL aircraft development led to a re-examination of this problem. The experimental investigations on jets in a transverse wind are compared in [8]. The complicated interaction between the jet and the incident flow which occurs at the point where the jet emerges into the transverse flow leads to a three-dimensional flow field, even if the jet axis remains in the x-y plane y = 0 [9, 10].

The variation of the jets for various inclination angles ϑ between the jet axis and the incident flow direction as well as at various velocity ratios V_j/V_∞ was investigated in [11 — 14]. Empirical parameters for the suction amounts, effective jet cross section area, and length of the potential flow have been determined from experimental investigations, and these can be used for a theoretical analysis of the jet [15]. Good results on the variations and cross section deformations of the jet in a cross wind are contained in [16 — 18]. /6

The present investigations aim to clarify the influence of temperature on the flow field of a round jet in a transverse wind. In order to have sufficiently large Reynolds numbers in the experiments, we investigated the jet propagation of a heated jet in the 3 meter wind tunnel of the DFVLR-AVA with various momentum ratios $\varphi = (\rho_j V_j^2)/(\rho_\infty V_\infty^2)$ in a cross wind.

The measurements were carried out between April 17, 1973 and May 11, 1973.

2. EXPERIMENTAL ARRANGEMENT

A jet nozzle is mounted on a sting balance carrier of the 3 meter wind tunnel of the DFVLR-AVA Goettingen [18]. It is equipped with heated air. The inclination angle ϑ with respect to the incident flow direction, that is the jet exit direction, can be changed. This first portion of the report contains measurements for the jet angle $\vartheta = 90^{\circ}$. The channel cross section of 3 x 3 m^2 makes it possible to investigate jet propagation for a nozzle diameter of D = 5 cm. In this way, it is possible to achieve wind tunnel velocities up to V_∞ = 50 m/sec and Reynolds numbers of $Re = \frac{V_\infty \cdot D}{\nu} \approx 1.7 \cdot 10^5$, referred to the jet diameter D = 5 cm.

2.1. The Nozzle Jet /7

The experimental installation is shown in Figure 1. The blower nozzle is mounted at a distance of 2 meters from the wind tunnel nozzle along the sting balance carrier of the test section. Figure 2 shows a photograph of the test installation in the 3 meter wind tunnel. The nozzle jet is blown out of an exchangeable nozzle (2 nozzle shapes), Figure 3, with an exit diameter of D = 5 cm. The expelled air is supplied by a screw compressor installation of the DFVLR-AVA at a pressure of p_t = 2.8 bar. The pressure is maintained constant by means of a pressure control valve. The pressurized air reaches the speed of sound at the narrowest point of the dosing valve. By displacing the central body of the dosing valve, it is possible to regulate the amount of expelled air. After this, the pressurized air flows through an electrical heater. It can be heated to temperatures of up to t_H = 400° C there. The control of the heating power is done by

means of a 400 kW Leonard unit, which is remotely controlled from the measurement cabin.

2.2. The Flow Field Measurement Installation

In our case of measuring the flow field, it was necessary to consider a large number of measurement points. Therefore a probe displacement unit (Figure 4) was constructed at the DFVLR-AVA and an automatic control was developed within this contract [19]. By means of a sequence control, it is possible to preselect 28 coordinates in a measurement test section (y coordinate here), which are then automatically executed by the displacement unit.

The flow field of the expelled air jet is measured using a nine hole directional probe (Figure 5). This probe makes it possible to measure the flow angle α_w, the side wind angle β_w, the total pressure g and the static pressure p. An electronic control unit automatically rotates the probe into the local flow direction α_w of the jet field (Figure 6). The side wind angle β_w is found from the pressure difference $\Delta p_\beta = p_a - p_s$ between two opposing pressure taps and the measured stagnation pressure $q_m = g_m - p_m$, using a calibration curve (Figure 7). The determination of the local stagnation pressure q_{oe} and of the static pressure p_{oe} for oblique blowing is also done using calibration curves (Figures 8 and 9). /8

The pressure measurement capsules have a measurement range of 0.5 bar for the total pressure g and 0.1 bar for the pressures Δp_α, Δp_β and p. The output voltages of these pressure measurement capsules are amplified and are averaged in integrating digital voltmeters over two-second intervals. There is a thermoelement installed in the probe, and its output voltage is amplified just as for the pressure measurement capsules. This is displayed on

a digital voltmeter. The measured values of pressure and temperature are recorded on an 8 channel punched tape. The experimental setup and the data collection unit is shown in Figure 1.

3. EXECUTION AND EVALUATION OF TESTS

In the present experimental test segment, we adjusted a velocity of the unheated nozzle jet of V_j = 180 m/sec and held the amount of expelled air constant. After controlling the wind tunnel velocity V_∞ in the range between 45 and 10 m/sec, we varied the velocity ratio $\psi = V_j/V_\infty = 4$ to 12 and the momentum ratio in the range ϕ = 16 to 64. The experiments with heated jets were only carried out after adjusting a constant temperature of $t_H \approx 350°$ C in the heater and $t_R \approx 300°$ C in the exhaust nozzle. The compressor installation can be used to investigate critical nozzle jets ($Ma_D = 1$) and overcritical nozzle jets ($Ma_D > 1$) by increasing the compressor pressure.

The flow field is measured in sections perpendicular to the channel axis at various displacements x/D from the center of the jet nozzle. Depending on the displacement, it is possible to measure an area of up to 1 m^2 using measurement point separations between 50 and 100 mm (Table 1).

A FORTRAN evaluation program was written for the electronic computer installation IBM 360-65 for evaluation of the measurements. The results are available in lists and cards. The computer program determines the resulting local velocity, its components V_x, V_y, and V_z in three coordinate directions and the flow angles α_w and β_w which these components make with the corresponding coordinate axes x, y, and z from the measured data (Figure 10).

Special plotting programs were designed for the CALCOMP plotter for representing the various results in a variety of ways. Mrs. Neher of the DFVLR-AVA computer center aided us in building the three-axis representation with engineering axionometric features.

4. RESULTS

4.1. Previous Reflections on the Jet Field Measurement

The theoretical results of [15] give the position of the jet axis for various velocity ratios V_j/V_∞ assuming that the jet sucks mass because of the turbulent friction, and that it encounters a resistance because of the incident flow. With these two assumptions, it is possible to explain the deformation and deflection of a jet. Earlier experimental investigations [17] indicate that the potential core of the jet is decomposed already after a path length of a few nozzle diameters. The jet is rapidly deflected in the direction of the wind tunnel flow because of intensive mixing. This is verified by the photographs of the jet made at various incident angle velocities, carried out before the present flow investigations (Figure 11). In the turbulent mixing regions, there are strong, approximately periodic fluctuations, which require a special investigation and special care when carrying out the measurements. Because of the quadratic relationship between the velocity and pressure, the time averaging of the velocity and the time averaging of the stagnation pressure lead to different results. For this reason, it is necessary to use pressure transducers with sufficiently small response time for measuring the jet field, so that the square root of the instantaneous value can be established which is required for determining the time average. /10

4.2. Velocity Distribution in a Cold and Hot Jet Without Cross Wind

Figures 12 to 15 show the dimensionless velocities plotted against the axis distance for cold ($\Theta = 1$) and hot ($\Theta = 2$) jets. At a distance of 0.1 D and 0.2 D from the nozzle exhaust points, we have rectangular velocity profiles for the conical and corrected nozzle, which do not differ from each other. As the distance z/D from the nozzle mouth is increased, the profiles become flatter. After z/D = 6, they are similar to Gaussian error functions, so that starting at this distance, z/D = 6, we can speak of a fully developed free jet. A comparison of the velocity profiles of cold ($\Theta = 1$) and hot ($\Theta = 2$) jets shows that there is a somewhat greater sidewise propagation of the hot jet, i.e., that the half-radius value for the hot jet is somewhat larger ($\Theta = 2$).

Figures 16 and 17 show the dimensionless velocities measured along the jet axis z. For conical and corrected nozzles, and for a cold jet ($\Theta = 1$), we find no differences in the velocity distribution along the jet axis z/D (Figure 16). In the case of the hot jet ($\Theta = 2$), the decrease in the axial velocity during the discharge process from the corrected nozzle occurs somewhat earlier than for the conical nozzle (Figure 3). Compared with /11
the results of [21], we find somewhat higher values of velocity along the axis (Figure 17).

4.3. Velocity Distribution in the Transverse Plane with a Cross Wind

In order to make the graphical representation of the velocities V, we made it dimensionless using the incident flow velocity V_∞ for our plotting program. These dimensionless velocities $c_V = V/V_\infty$ are shown in Figures 18 to 23 and are indicated as lines of constant velocity c_V = const, the so-called isotachs. In order

to make clear the distance to the nozzle, we also show it to scale in the diagrams.

The isotachs very clearly indicate the deformation of the nozzle jet under the effect of the cross flow. Already in [7], it was shown how the circular jet cross section is deformed into a kidney-shaped cross section in the case of cross flow, because a non-uniform pressure field is produced by the flow around the jet. In this deformation of the jet cross section, depending on the magnitude of the momentum ratio ϕ, a vortex pair is produced already after a short distance of a few nozzle diameters, which is caused by the transverse flow. This is similar to the flow around a cylinder at incidence.

One obtains an even clearer representation of the dissolution of a jet in a cross flow by showing the velocity components V_y/V_∞ and V_z/V_∞, which are obtained by projecting velocity vectors $\underline{V}/V_\infty$ onto the transverse plane (y-z plane) (Figures 24 to 31). This was done using a plotter program for the CALCOMP plotter. In this representation, we also show the nozzle exhaust to scale as well as a comparison vector in the z direction having the magnitude $V_z/V_\infty = 0.1$. These are used as reference quantities.

These vector diagrams very clearly show the position and magnitude of the vortex pair rotating in opposite directions, which can be found already at a short distance from the nozzle ($x/D = 7$) and for small momentum ratios $\phi = 16$ (Figure 24). /12
These vortices absorb an axial momentum from the jet and flow in the direction of the jet axis (Figure 25), whereby their dimensions increase. In the far field of the jet ($x/D = 15$), according to Figures 25, 27, 29, and 31, it seems that the jet disappears, which the preceding isotachs also show (Figures 18 to 23). The flow field of the nozzle jet is then only characterized by a vortex pair, which only starts to disintegrate after a long distance due to the effect of friction.

If one compares the vector diagrams for the cold jet (Figures 26 and 27) with the corresponding diagrams for the hot jet (Figures 28 and 29), we find that the structure of the jet cross section in the form of a vortex pair rotating in opposite directions is maintained. However, it is found that, for the same velocity ratio $\psi = 8$, the vortex centers of the cold nozzle jet have separated more from the nozzle exit point in the z direction, and therefore, the velocity ratio ψ is not a similarity parameter for the flow simulation of hot gas jets.

A comparison of the vortex fields of cold (Figures 26 and 27) and hot jets (Figures 30 and 31) with the same momentum ratio $\phi = 64$ indicates the same variation in the jet axis and the same position of the vortex centers with respect to the z axis. The differences between both jet fields seem to be characterized by a somewhat greater propagation of the vortex fields for the hot jet. According to these preliminary results, it seems that the computation of the momentum ratio

$$\phi = (\rho_j V_j^2)/(\rho_\infty V_\infty^2)$$

seems to be important for jet simulation.

4.4. Flow Direction in the Symmetry Plane of the Jet

The importance of the momentum ratio ϕ for simulation of hot gases is confirmed by measurement of the flow angle α_w. For the graphical representation of the flow angle α_w of the symmetry plane of the flow field ($y = 0$), they are referred to the nozzle angle ϑ and Figures 32 and 33 show the dimensionless jet inclinations for $\varphi = \alpha_w/\vartheta$ as a function of the dimensionless coordinate z/D of the jet cross section. /13

The isotach diagrams (Figures 18 to 23) show a fast decrease in the velocity profiles with path length. However, there is a well developed directional field up to large nozzle distances x/D = 15. We find that, for the same momentum ratio of hot and cold jets, the distribution and distance from the nozzle exit point z of the directional field is approximately the same. On the other hand, the directional fields of cold and hot jets for the same velocity ratio $\psi = 8$ have different magnitudes and positions.

4.5. Three-Dimensional Representations

The representation of the flow field in two dimensions is only a partial view of the relationships which occur during jet mixing with the parallel flow. Therefore, Figures 34 to 41 give a three-dimensional representation in the form of an isometric method of representation. In these figures, the dimensionless component $(V_x - V_\infty)/V_\infty$ of the normal velocity on the y-z plane, represented by the coordinates y/D and z/D, is shown.

The velocity distributions for a small momentum ratio $\phi = 16$ in the two measured intersection planes x/D = 7 and 15 (Figures 34 and 35) only show a developed wake field behind the nozzle jet and the nozzle jet can only be detected in the form of an overvelocity $(V_x - V_\infty)/V_\infty$ at the small distance x/D = 7. For the momentum ratio $\phi = 32$, one finds a characteristic velocity distribution for the mixing of a subsonic jet in a cross flow (Figures 38 and 39).

This flow field is characterized by a semicircle region with an overvelocity of up to 30%, which includes the wake region in the symmetry plane (y/D = 0). The maxima of these overvelocities approximately agree with the centers of the opposing vortex pairs shown in the vector representation (Figures 24 to 31). The /14

comparison of the velocity fields of the cold (Figures 36 and 37) and of the hot (Figures 40 and 41) jet for a momentum ratio of $\phi = 64$ shows that there is good agreement of the velocity distribution $(V_x - V_\infty)/V_\infty$ in comparable measurement sections.

4.6. Comparison of Results using the Theory of Jet Paths

In Figure 42 is shown the path of the jet core of a cold nozzle jet in a cross wind for the velocity ratios $\psi = 4.3$ and 8.1, according to the theory [14]. Comparable experimental results [22] are also shown in these diagrams.

The vortex pairs detected in this investigation clearly show the vortex course, and their distances z/D and x/D from the nozzle exit point are shown as measurement points in Figure 42. Compared with the theoretical and experimental paths of the jet core, the vortex cores experience a greater deflection by the cross wind. Here again, it can be found that the same velocity ratio ψ alone does not bring about the same position of the vortex core, when the jet temperature changes. On the other hand, the position of the vortex core of cold and hot jets remains the same for the same momentum ratio $\phi = 64$.

5. SUMMARY

The experimental investigations on cold ($\Theta = 1$) and hot ($\Theta = 2$) air jets in cross winds for jet velocity to cross wind velocities of $\psi = V_j/V_\infty = 4.8$ and 11.3 have shown that the well-known initial kidney-shaped deformation of the jet cross section due to the normal cross wind very soon leads to the formation of a pair of vortices rotating in opposite directions. This vortex pair limits the deflected engine jet to the side with respect to its symmetry plane. The velocity along the "jet core" is

described by the theory and decreases rapidly, so that at a distance of about 7 nozzle diameters behind the center of the nozzle, less than 10% of the different velocity between the jet and the cross flow can be measured. On the other hand, higher velocities occur in the vortex cores up to large distances, as measurements have shown at x/D = 15.

For the same jet to cross wind velocity ratio, the heating of the jet brings about a larger deflection of the jet and the vortex cores. Compared with the velocity fields found for the same exhaust jet to cross flow momentum ratio, it is found that the positions of the jet core and the vortex pair are essentially conserved, even though the velocity vectors in the vicinity of the vortex cores would lead one to conclude that there was a greater jet expansion.

6. REFERENCES

/16

1. Kennedy, V. S., and J. A. Mihursky. Bibliography of the Effects of Temperature in the Aquatic Enviornment. Submitted to Hearings on Thermal Pollution - 1968, before the Committee on Air and Water Pollution, U. S. Senate, February 1968, Part I, GPO, pp. 471-568.

2. Parker, F. L., and P. A. Krenkel. Physical and Engineering Aspects of Thermal Pollution. CRC Critical Reviews in Environmental Control, Vol. I, 1970, pp. 101-192.

3. Williams, J., and Maurice N. Wood. Aerodynamic Interference Effects with Jet-Lift V/STOL Aircraft under Static and Forward Speed Conditions. RAE Technical Report No. 66403, 1966.

4. Fuetterer, H., and L. Harms. Jet Interference Measurements on a VTOL Model with Jet Simulation by Fans. AGARD Conference Proceedings 22, 1967. pp. 17/1 - 17/26.

5. Kush, E. A., and J. A. Schetz. Liquid Injection into a Supersonic Flow AIAA Journal, Vol. 11, 1973, pp. 1223 - 1224.

6. Schetz, J. A., and F. S. Billig. Penetration of Gaseous Jets Injected into a Supersonic Stream. Journal of Spacecraft and Rockets, Vol. 3, 1966, pp. 1658-1665.

7. Chang, H.-C. Die Aufrollung eines zylindrischen Strahles durch Querwind (The Rolling Up of a Cylindrical Jet Caused by the Cross Wind). Dissertation, University of Goettingen 1942, pp. 1-52.

8. Margason, R. J. Je-Wake Characteristics and Their Induced Aerodynamic Effects on V/STOL Aircraft in Transition Flight. NASA SP-218, 1969, pp. 1-18.

9. Bradbury, L. The Static Pressure Distribution around a Circular Jet Exhausting from a Plane Wall into an Airstream. British Aeronautical Research Council Current Paper 822, 1965.

10. Crowe, C., and H. Riesebieter. An Analytic and Experimental Study of Jet Deflection in a Cross Flow, Vortrag beim AGARD Fluid Dynamics Panel Meeting, Goettingen, AGARD Conference Proceedings No. 22, 1967, pp. 16/1-16/19.

11. Gordier, R. L. Studies on Fluid Jets Discharging Nasuall /17
Into Mowing Siguid. University of Minnesota, St. Anthony Falls, Hydraulic Labs, Technical Paper No. 28, Series B, 1959.

12. Margason, R. J. The Path of a Jet Directed at Large Angles to Subsonic Free Stream. NASA TN D-4919, 1968.

13. Platten, J. L., and J. F. Keffer. Deflected Turbulent Jet Flows. Journal of Applied Mechanics, Vol. 38, 1971, pp. 756-758.

14. Seidel, M. Investigations on the Influence of an Inclined Engine Jet on the Aerodynamic Properties of a Control Surface. ZfW, Vol. 19, 1971, pp. 13-29.

15. Schmitt, H. Deflection of a Round Turbulent Free Jet in A Cross Wind. DFVLR-AVA Report 061-72 A 24, 1972.

16. Abramovich, G. N. The Theory of Turbulent Jets, MIT Press, Cambridge, Massachusetts, 1963.

17. Keffer, J. F., and W. D. Baines. The Round Turbulent Jet in a Cross Wind. Journal of Fluid Mechanics, Vol. 15, Part 4, 1969, pp. 481-496.

18. Kamotani, Y., and I. Greber. Experiments on a Turbulent Jet in a Cross Flow. AIAA Journal, Vol. 10, 1972, pp. 1425-1429.

19. Fuetter, H., D. Mehme, and F. W. Riegels. Measurement Technology, Data Processing, and Data Collection at Large Wind Tunnels of the Aerodynamic Test Facility at Goettingen. Yearbook 1970 of the DGLR, 1971, pp. 166-185.

20. Mehmel, D. Investigations on the Flow Field of a Jet in an Oblique Cross Wind and a Parallel Flow. AVA Report 67 A 53, 1967.

21. Corrsin, S. Further Experiments on the Flow and Heat Transfer in a Heated Turbulent Jet. NACA Report 998, 1950.

22. Laurence, J. Intensity, Scale, and Spectra of Turbulence in Mixing Region of Free Subsonic Jet. NACA Report 1292, 1956.

23. Jordinson, R. Flow in a Jet Directed Normal to the Wind. ACR, R + M 3074, 1958.

Translated for National Aeronautics and Space Administration, under Contract No. NASw-2483, by SCITRAN, P. O. Box 5456, Santa Barbara, California 93108.

TABLE 1

MEASUREMENT PROGRAM*

MR	ψ	ϕ	x/D	Θ	Figure Number
1 - 3	4 - 12	16 - 64	0 - 15	1 - 2	12, 13, 14, 15, 16, 17
4 - 12	4	16	15	1	25, 33, 35
13 - 20	4	16	7	1	24, 32, 34
21 - 34	8	64	7	1	18, 26, 32, 36
35 - 55	8	64	15	1	19, 27, 33, 37
72 - 87	8	32	15	2	21, 29, 33, 39
88 - 99	8	32	7	2	20, 28, 32, 38
100 - 112	11,3	64	7	2	22, 30, 32, 40
113 - 120	11,3	64	15	2	23, 31, 33, 41

* Translator's Note: Commas in numbers indicate decimal points.

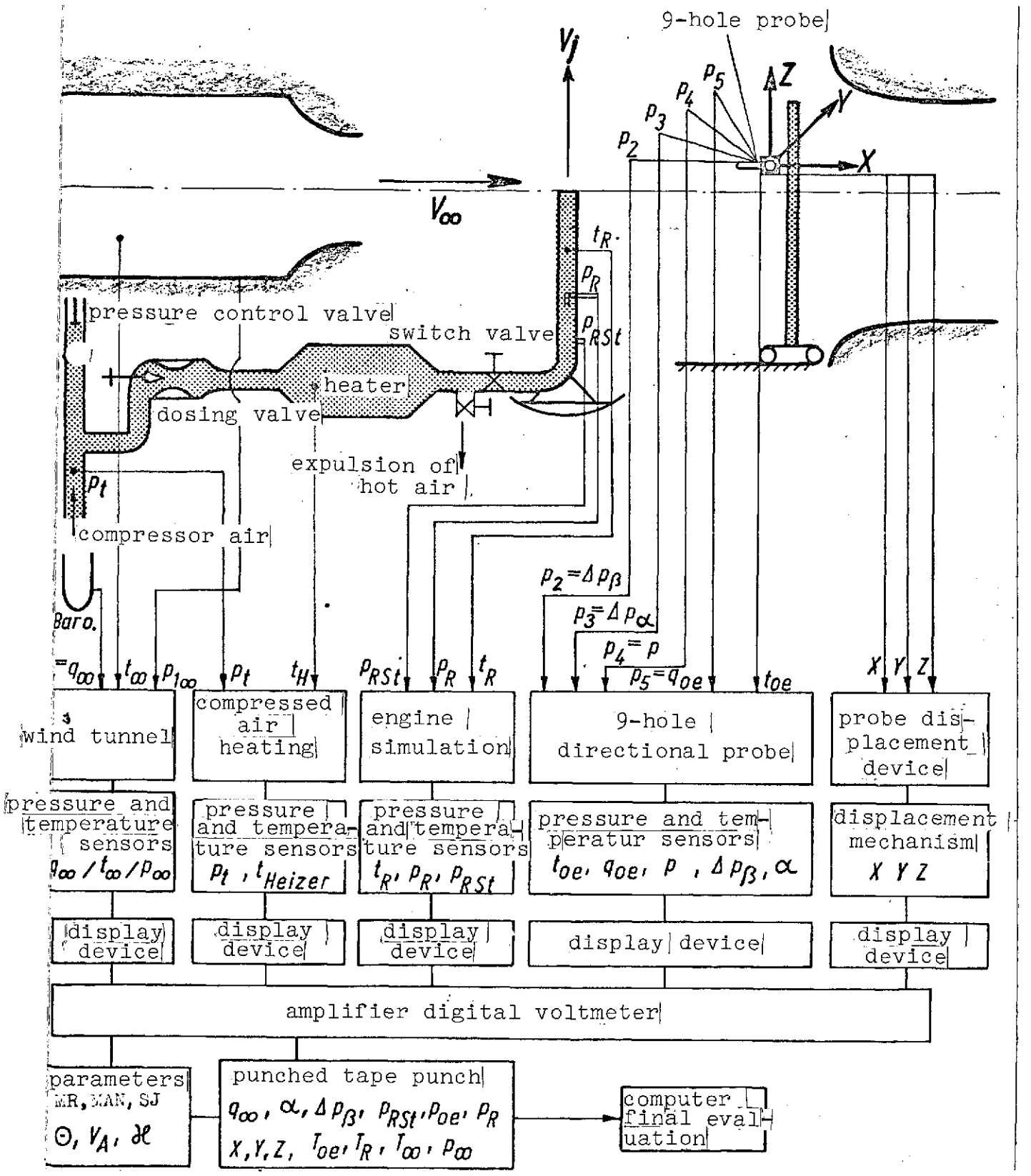

Figure 1. Experimental configuration for a jet simulation

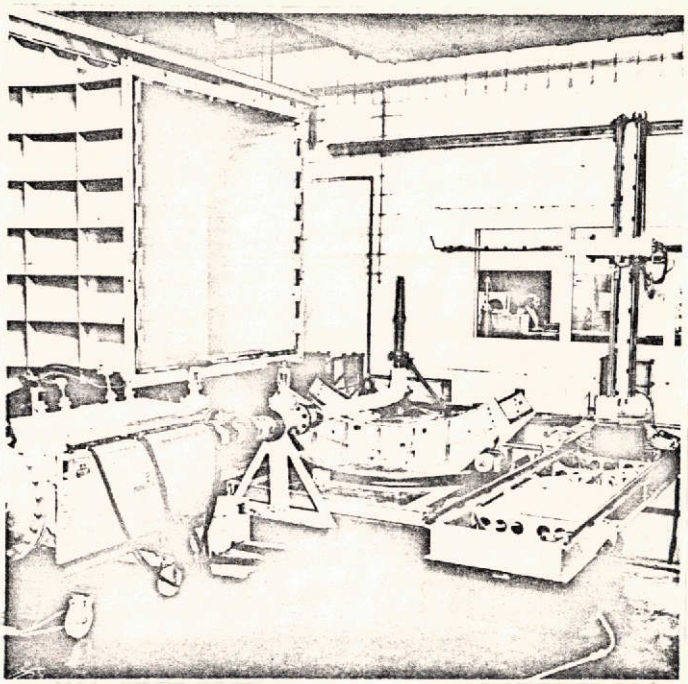

Figure 2. Photograph of the test installation in the 3-meter wind tunnel

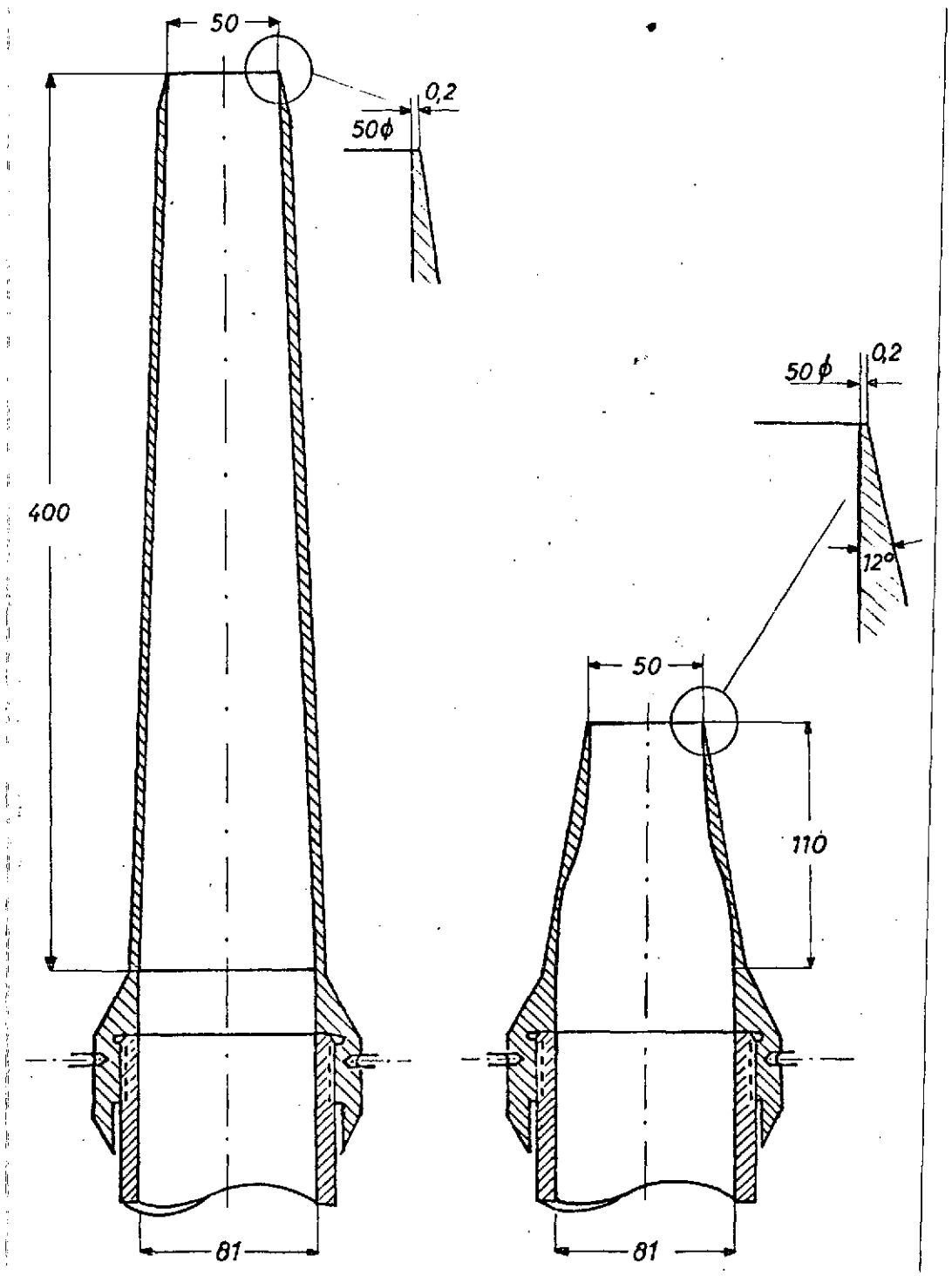

a) Conical nozzle b) Corrected nozzle

Figure 3. Exchangeable exhaust nozzles

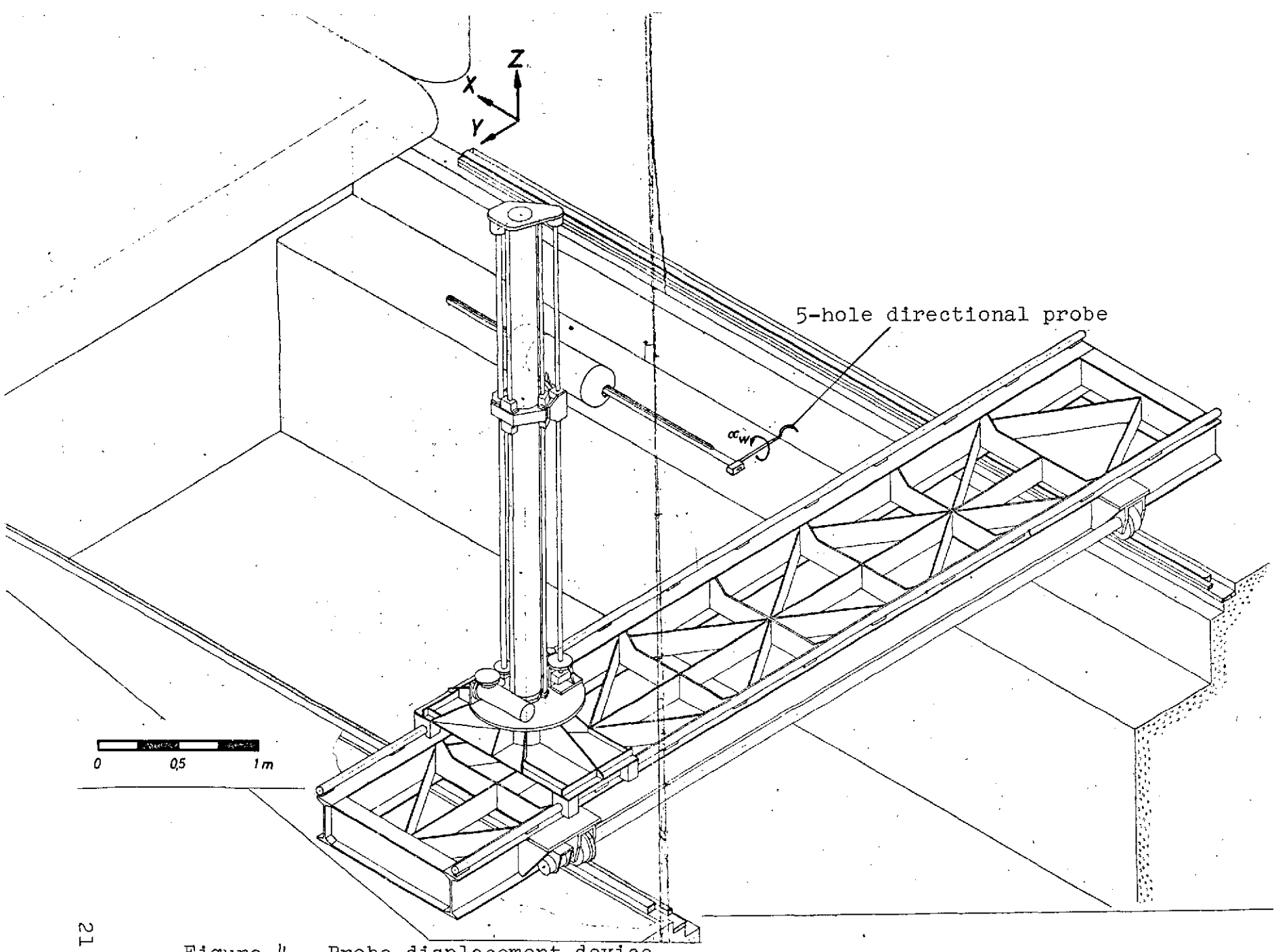

Figure 4. Probe displacement device.

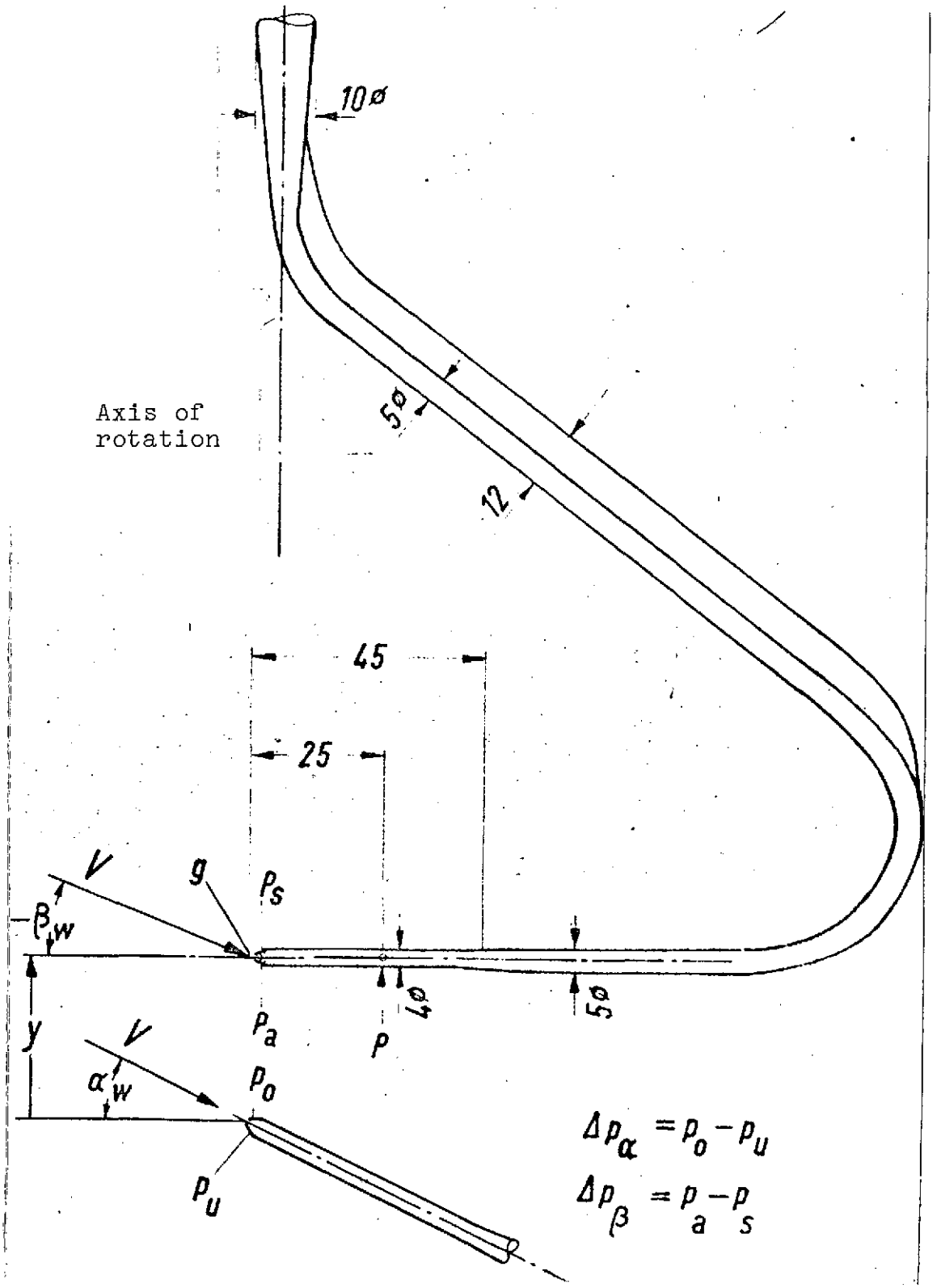

Figure 5. Nine-hole directional probe

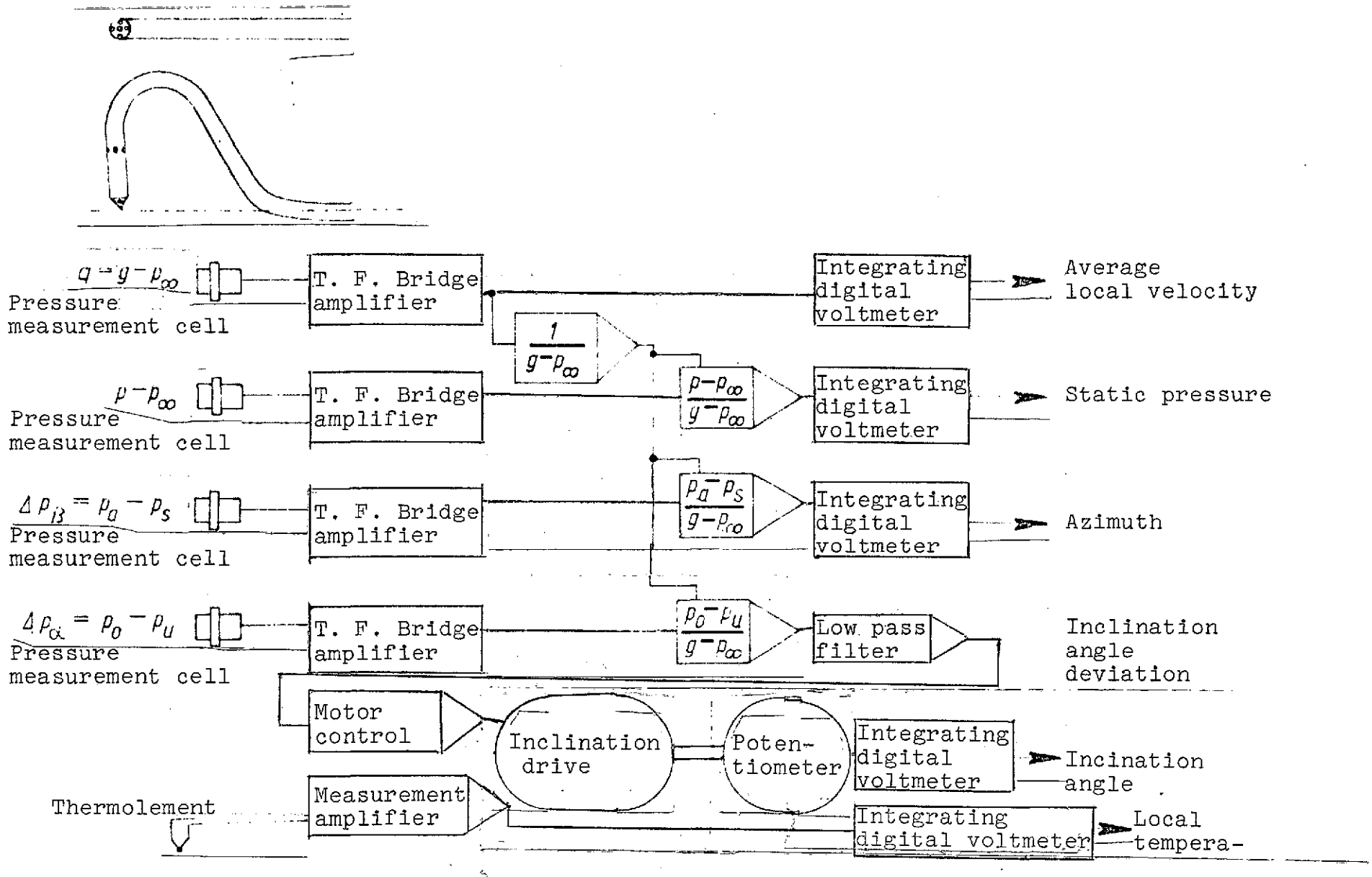

Figure 6. Flow field measurement in wind tunnel using 9-hole probe

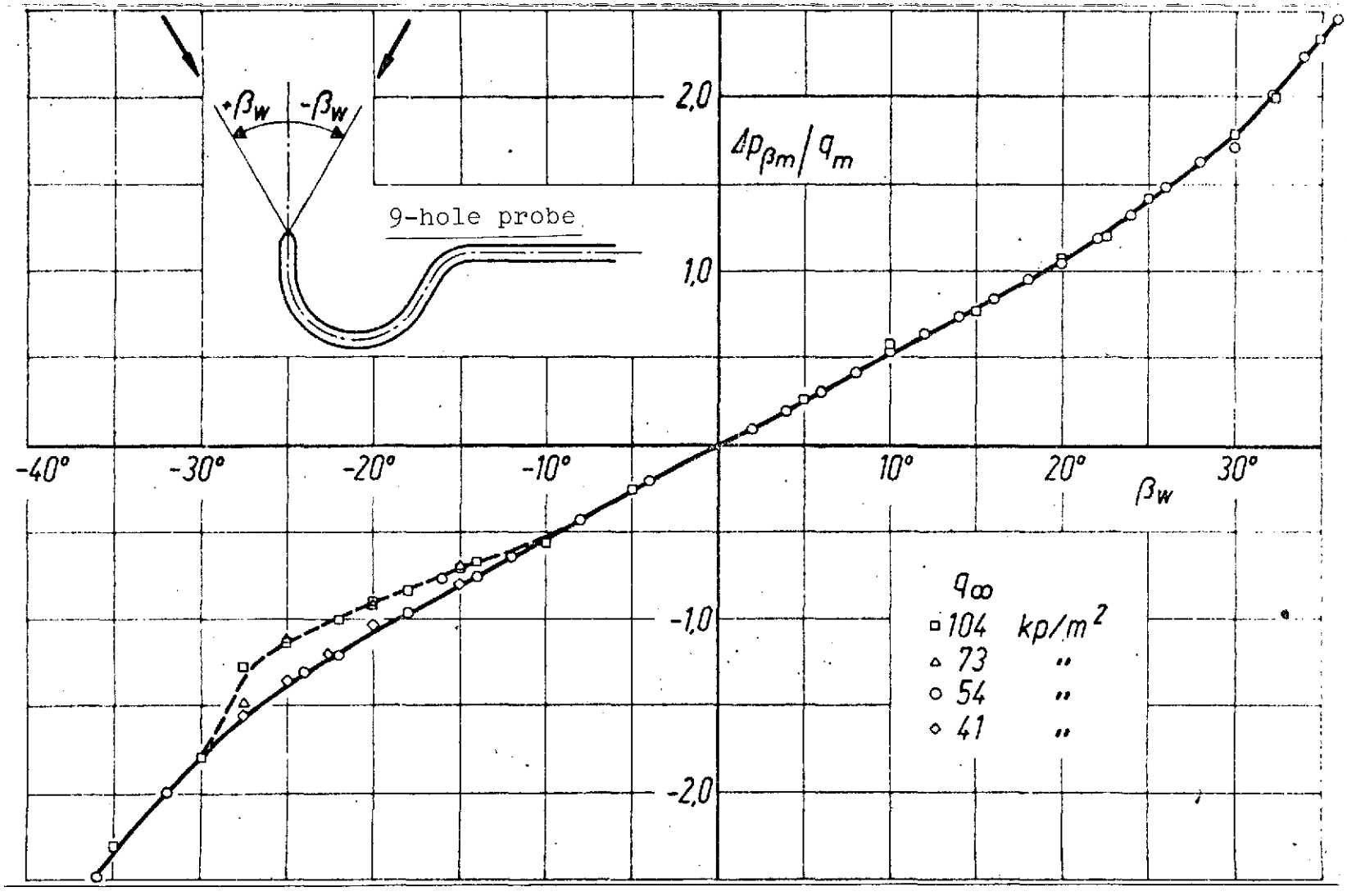

Figure 7. Calibration curve for the side wind angle

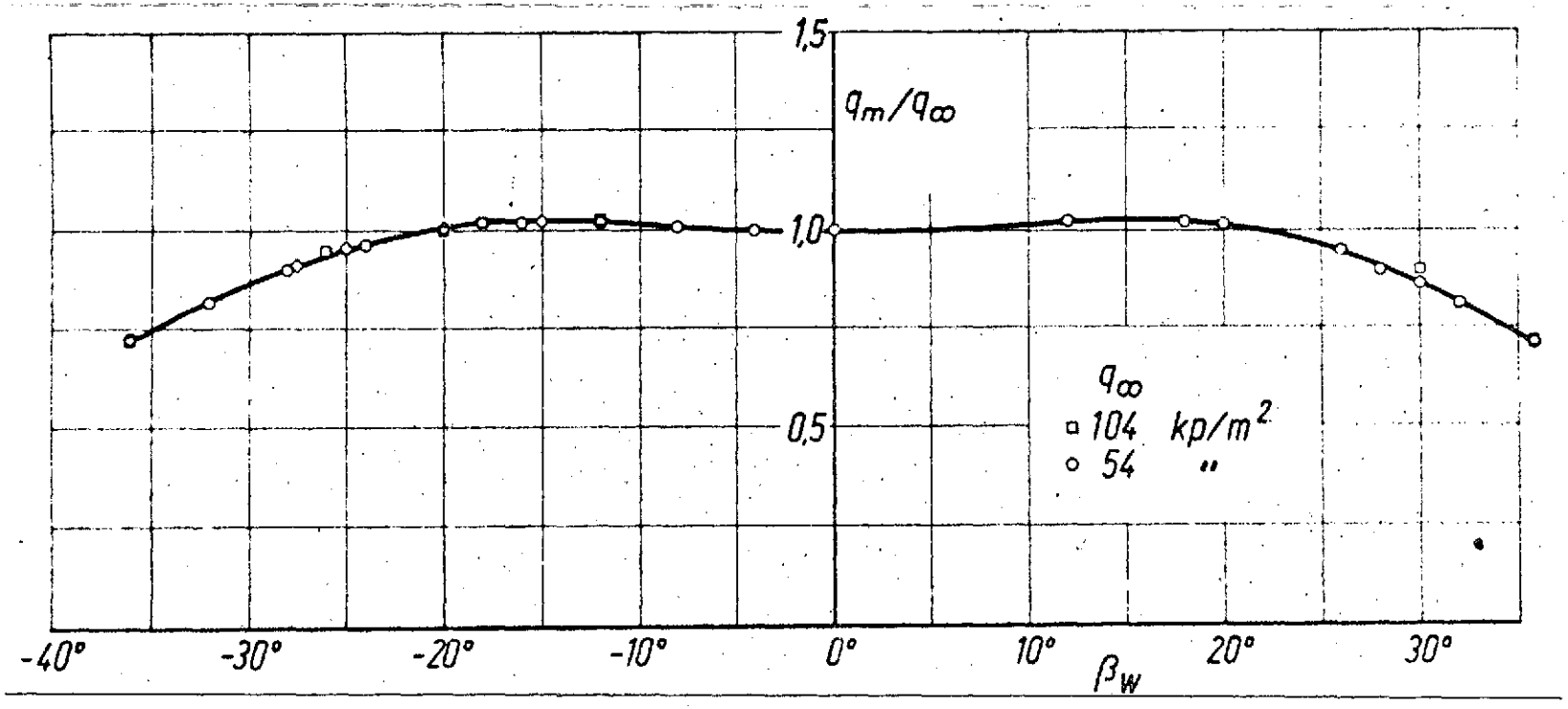

Figure 8. Calibration curve for the stagnation pressure

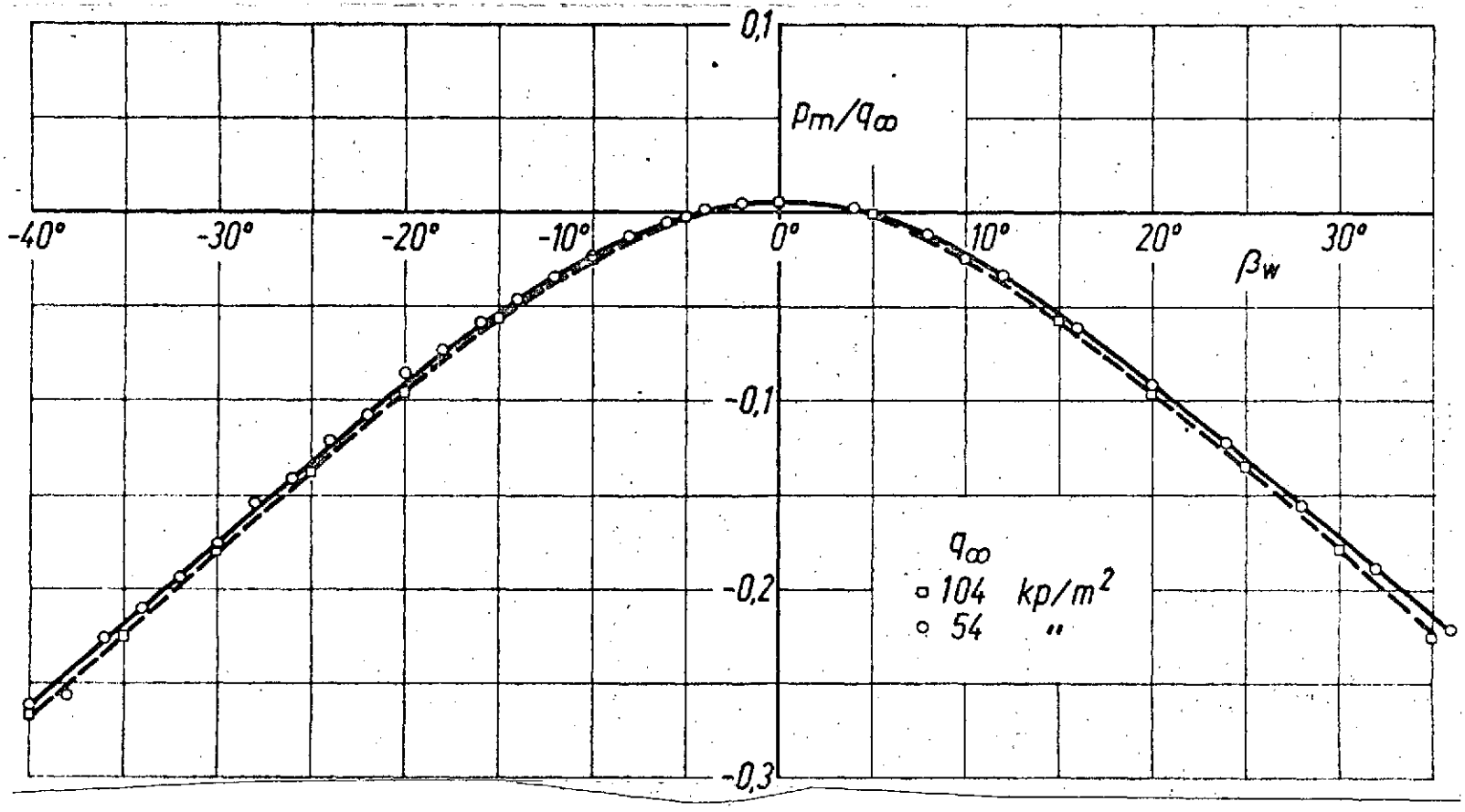

Figure 9. Calibration curve for static pressure

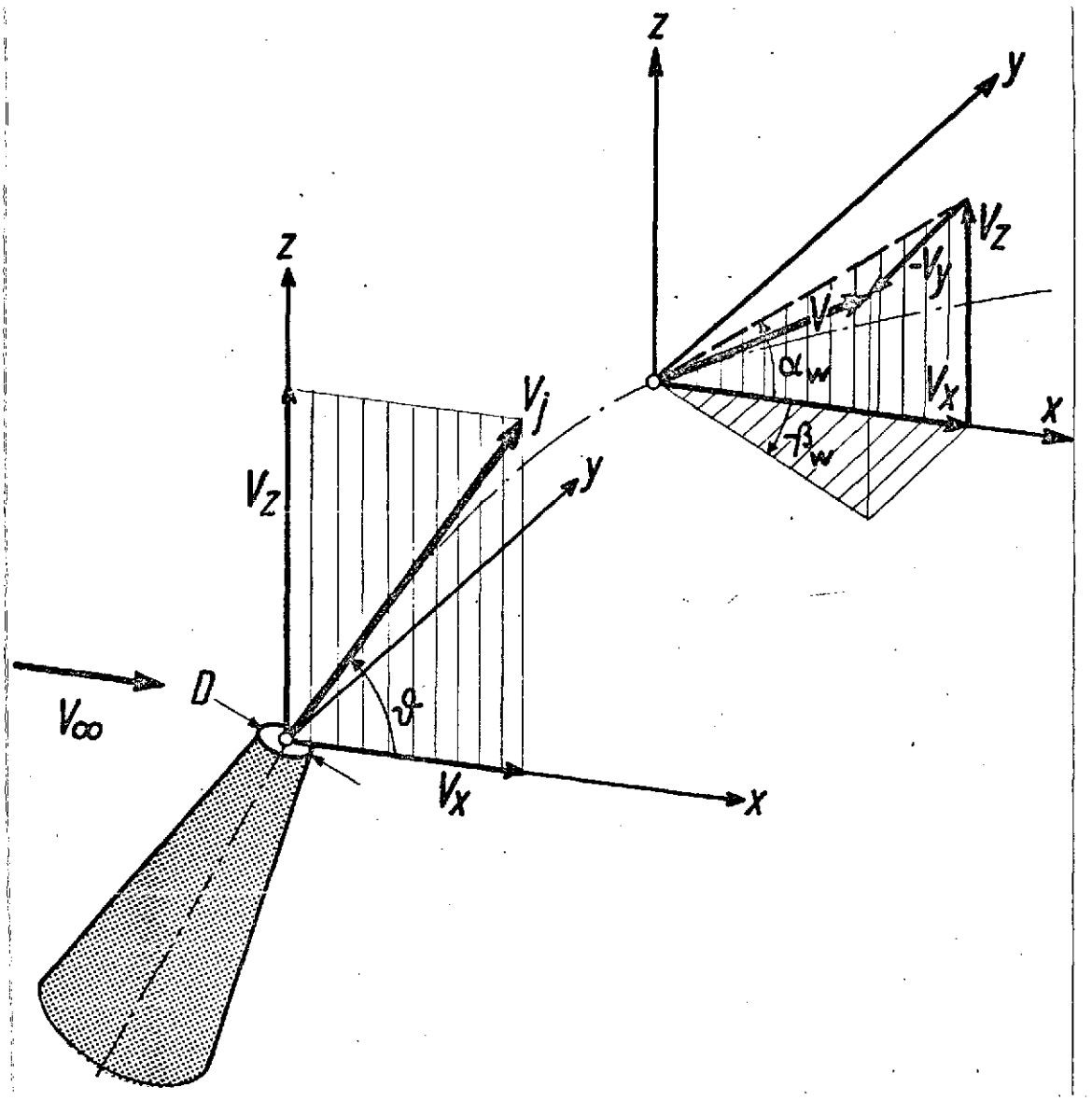

Figure 10. Axis system and notation

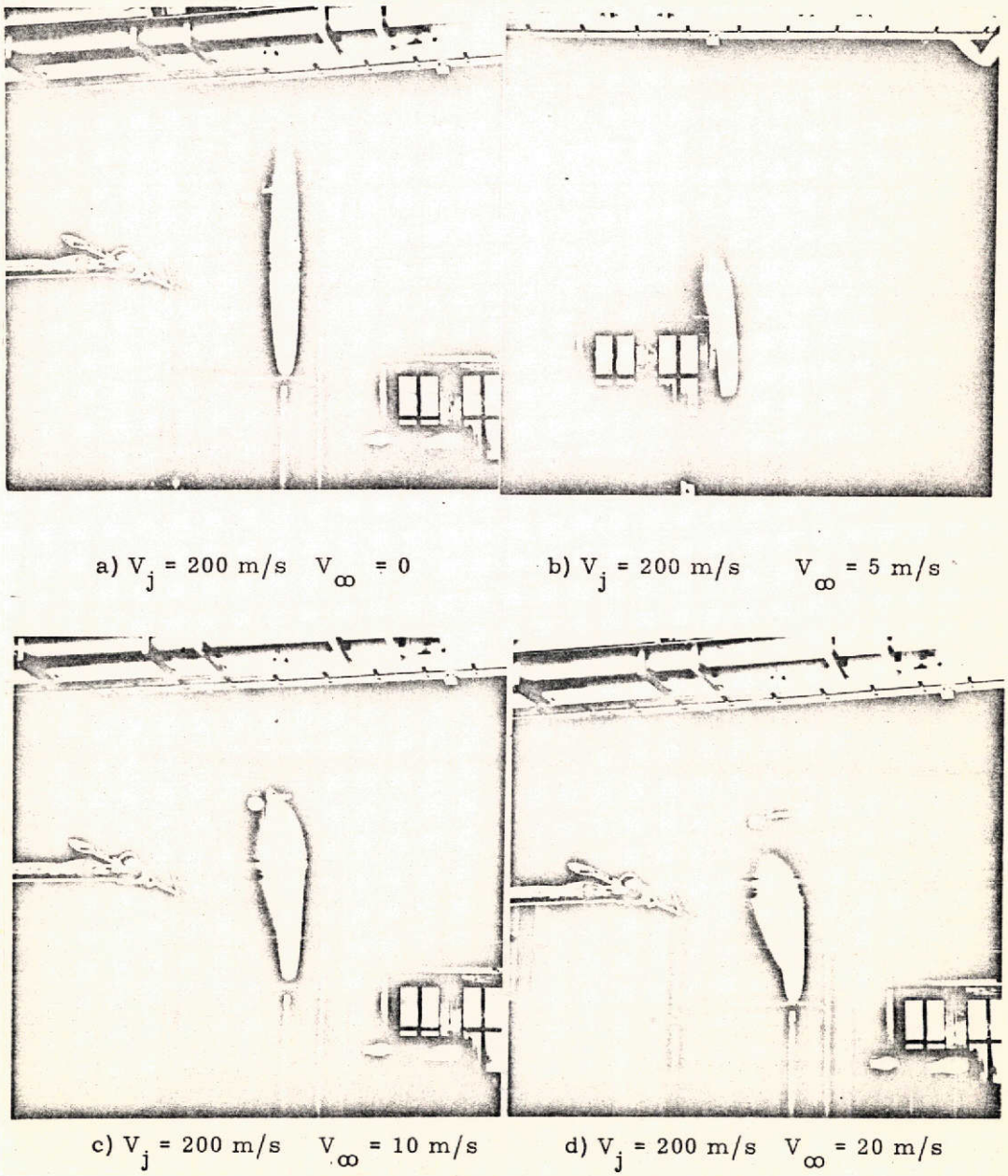

Figure 11. Flow photographs of the jet for various transverse velocities

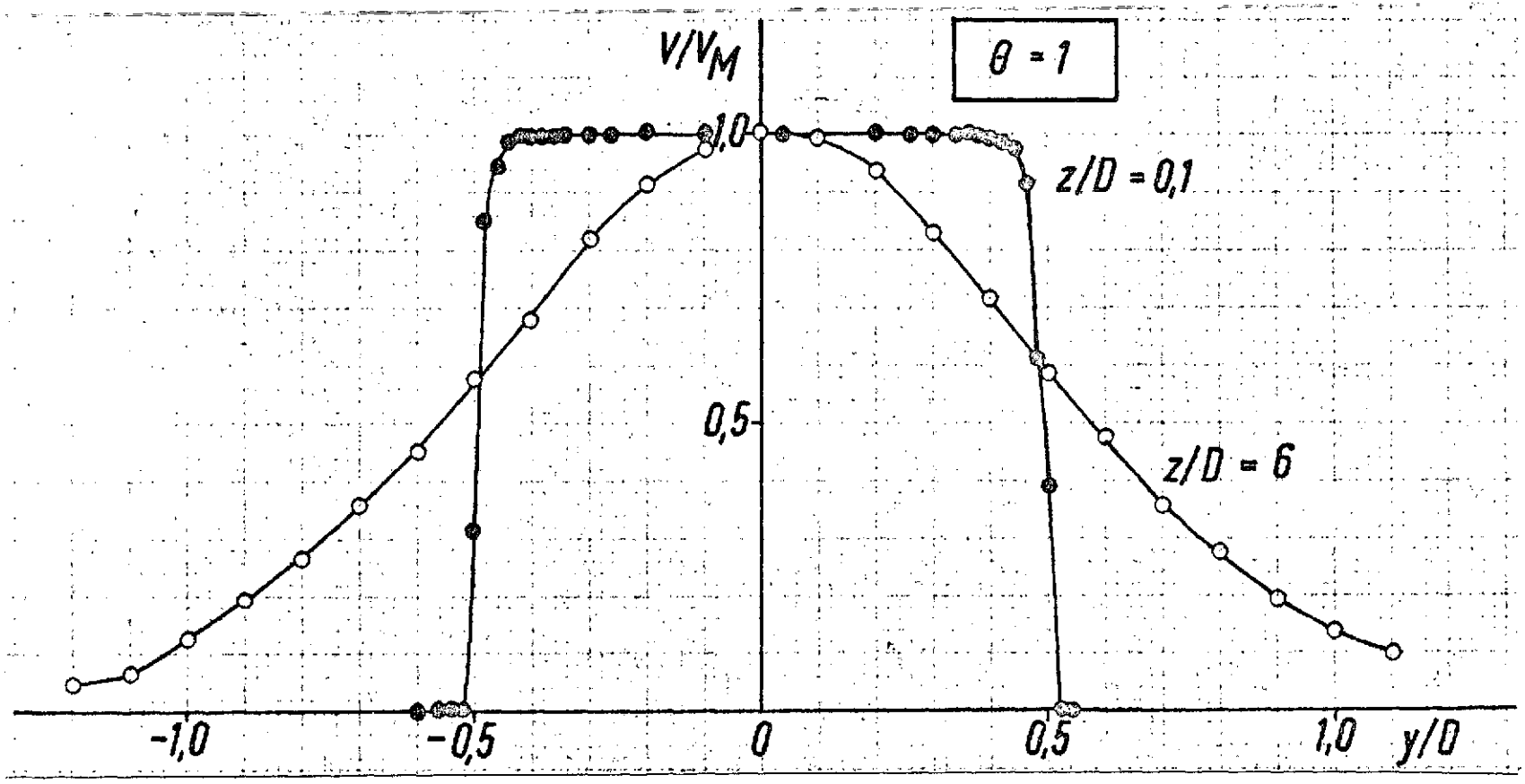

Figure 12. Velocity distributions in the cold jet of the conical nozzle

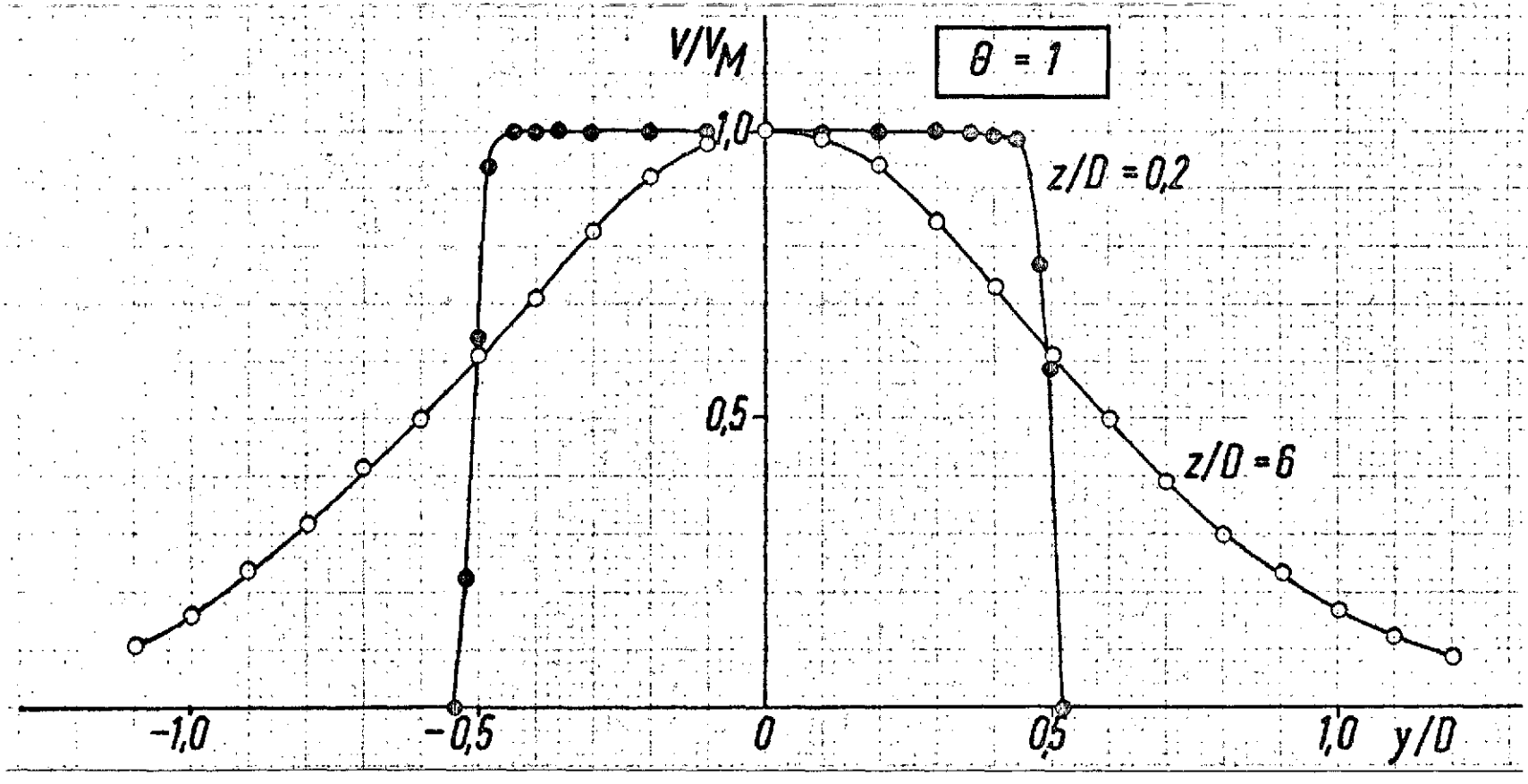

Figure 13. Velocity distribution in the cold jet of the corrected nozzle.

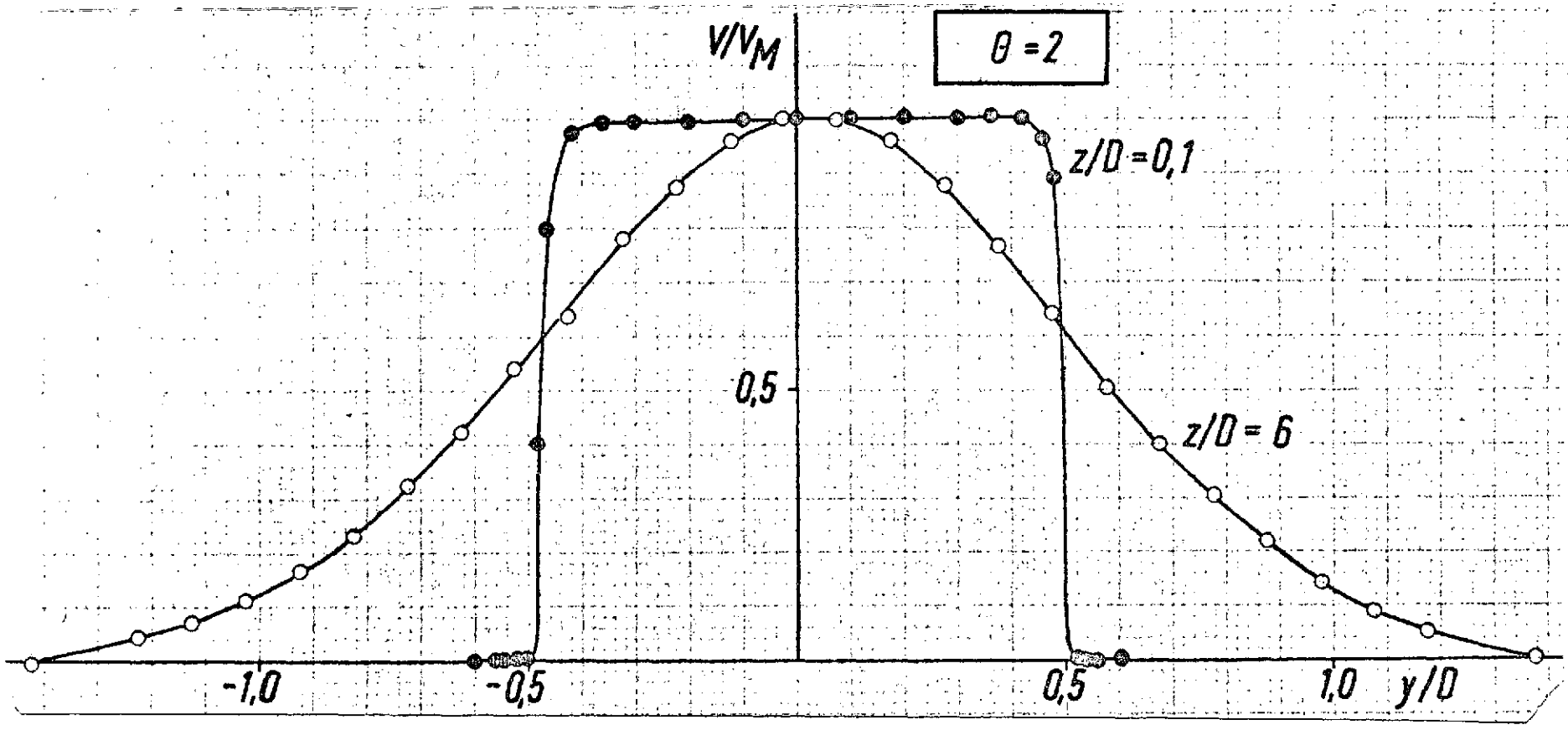

Figure 14. Velocity distribution in the hot jet of the conical nozzle

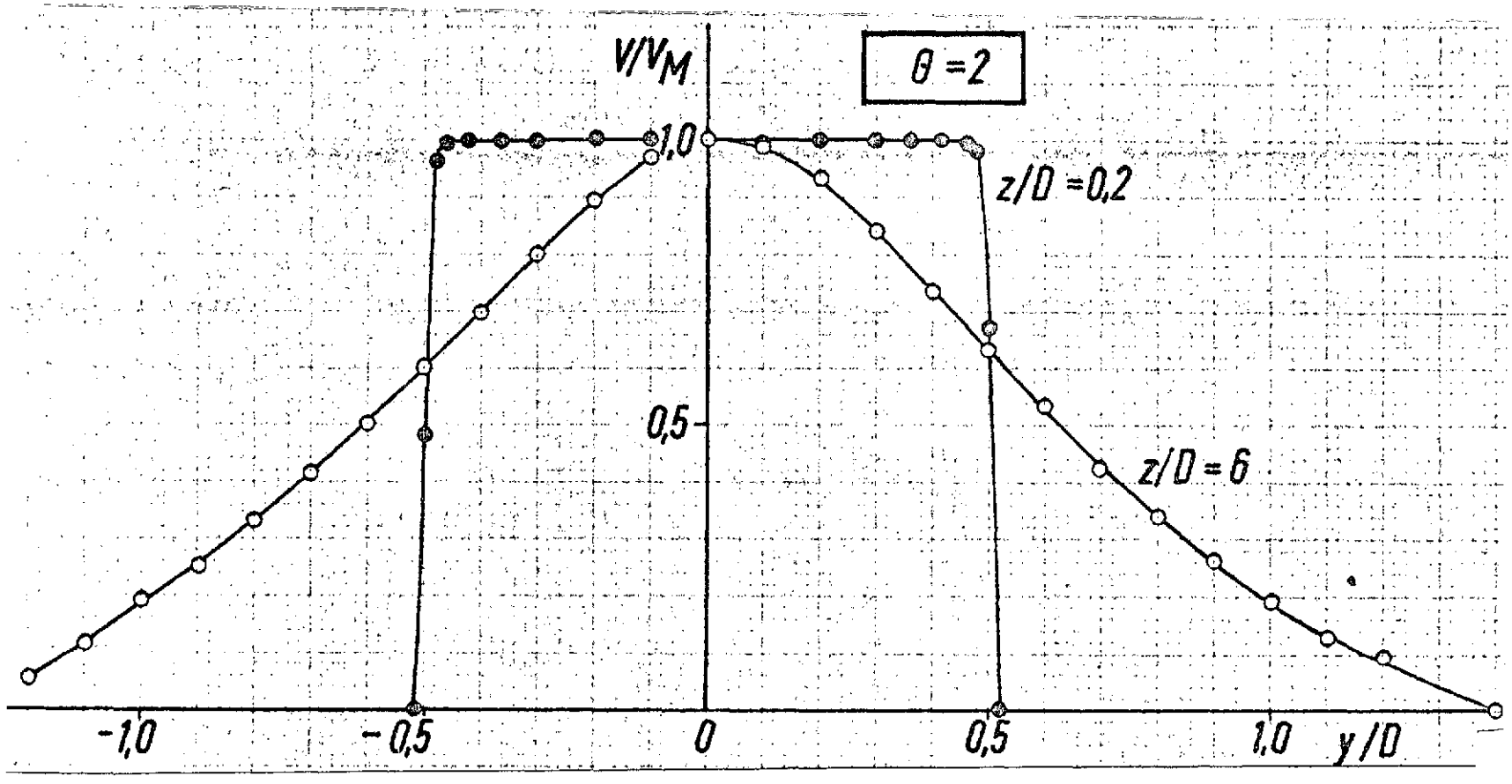

Figure 15. Velocity distribution of the hot jet of the corrected nozzle

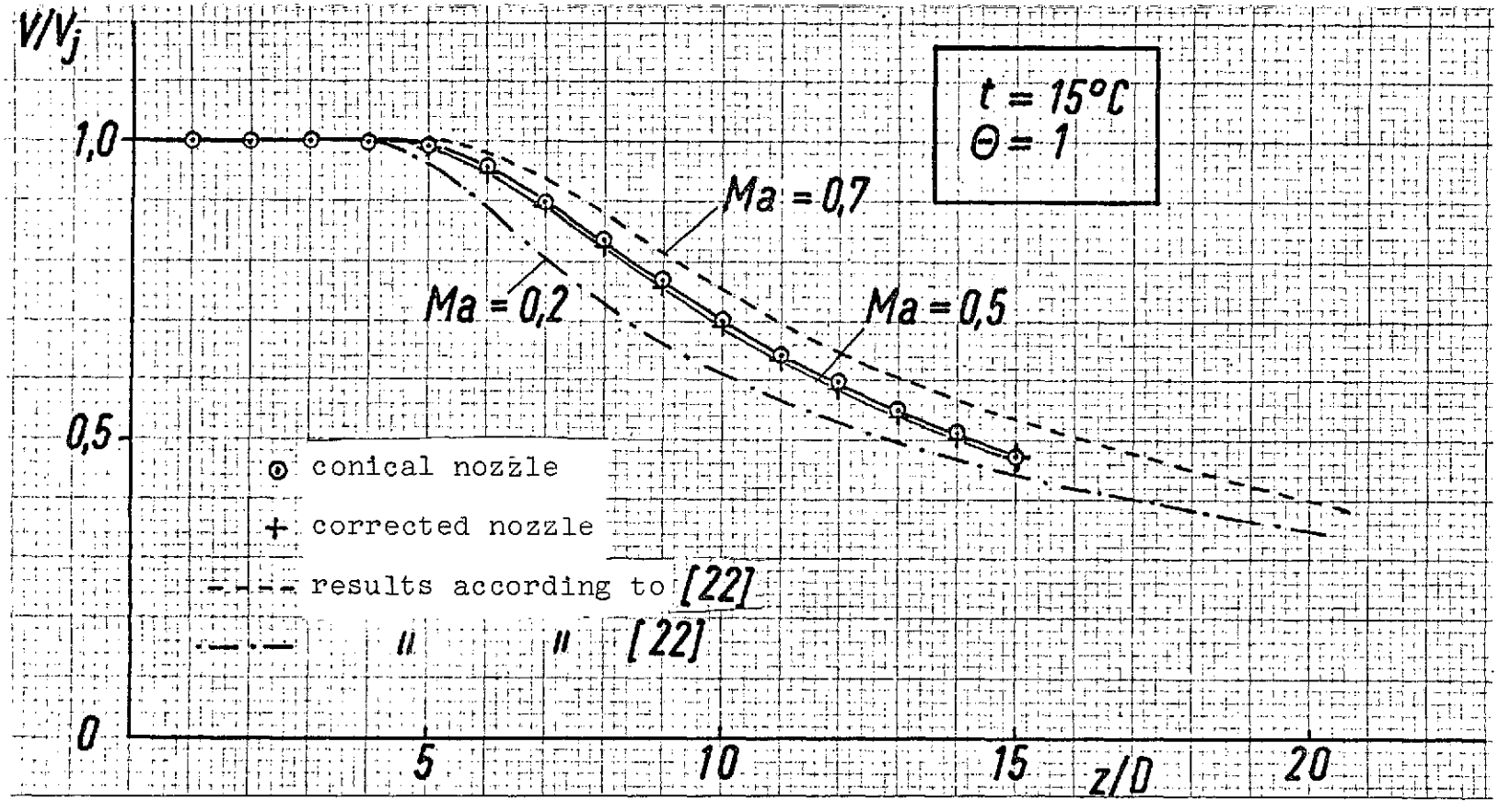

Figure 16. Velocity distribution along the jet axis, influence of Mach number

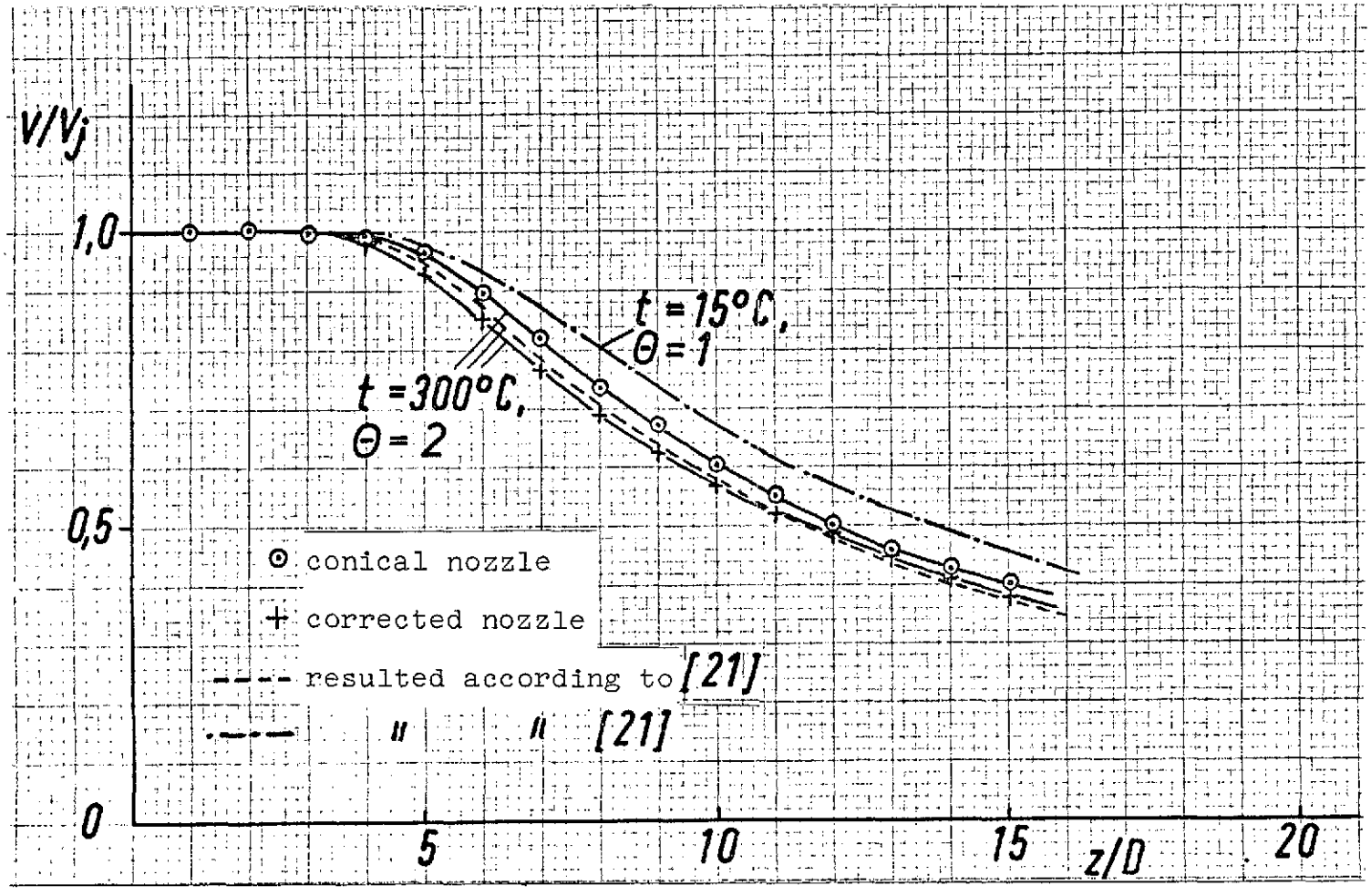

Figure 17. Velocity distribution along the jet axis, influence of jet temperature

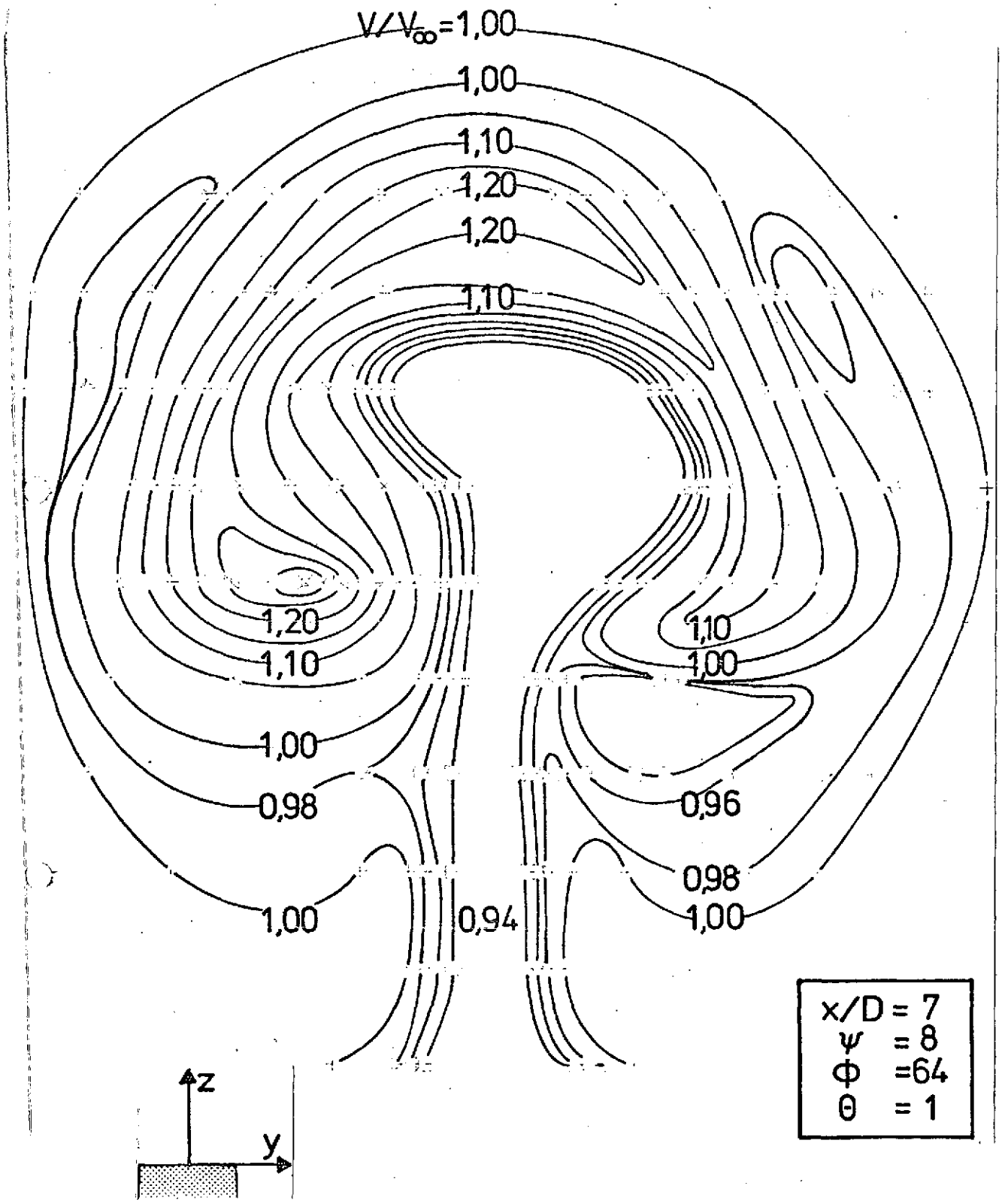

Figure 18. Velocity distribution in the transverse plane (y-z plane) of the cold jet

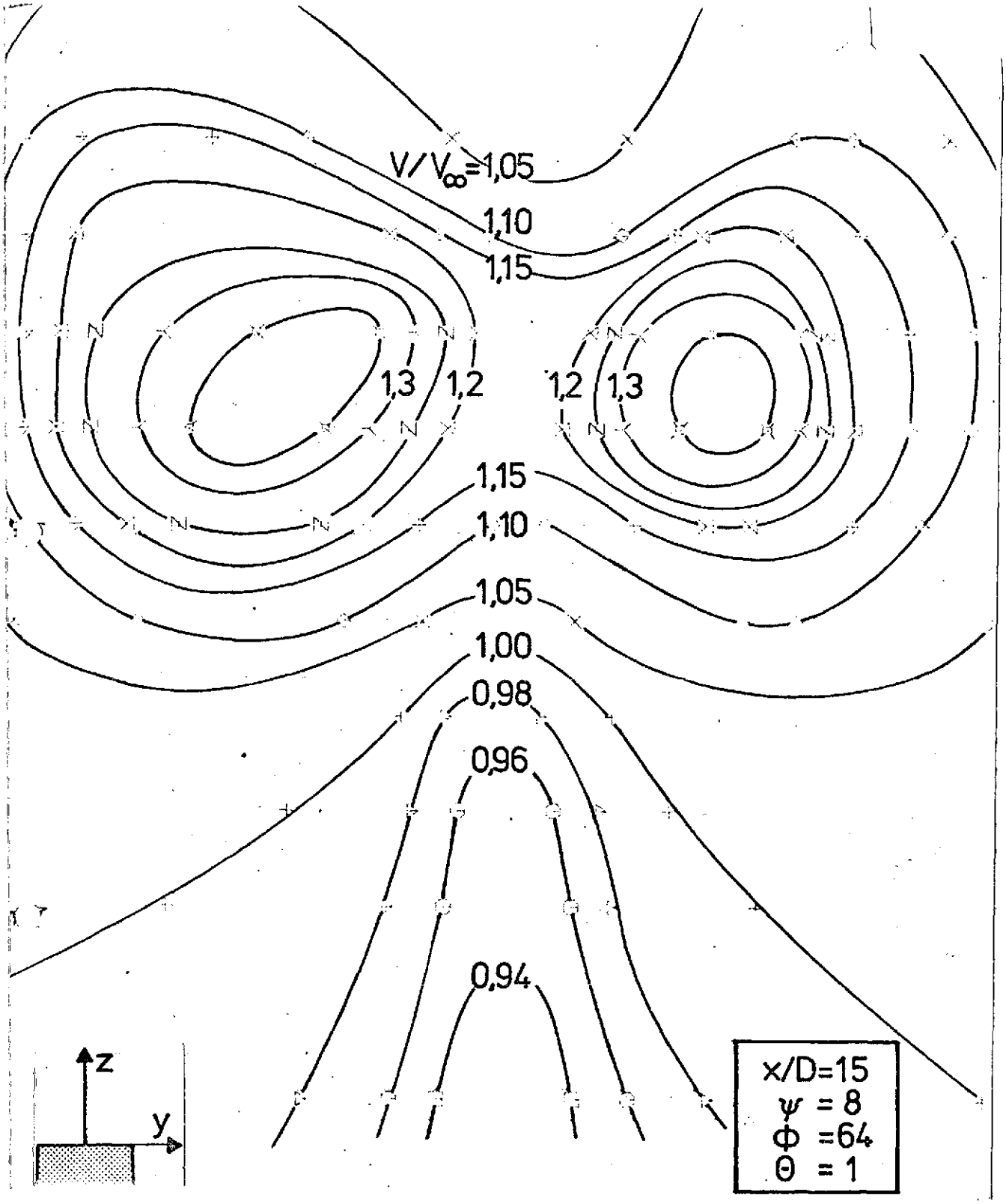

Figure 19. Velocity distribution in the transverse plane (y-z plane) of the cold jet

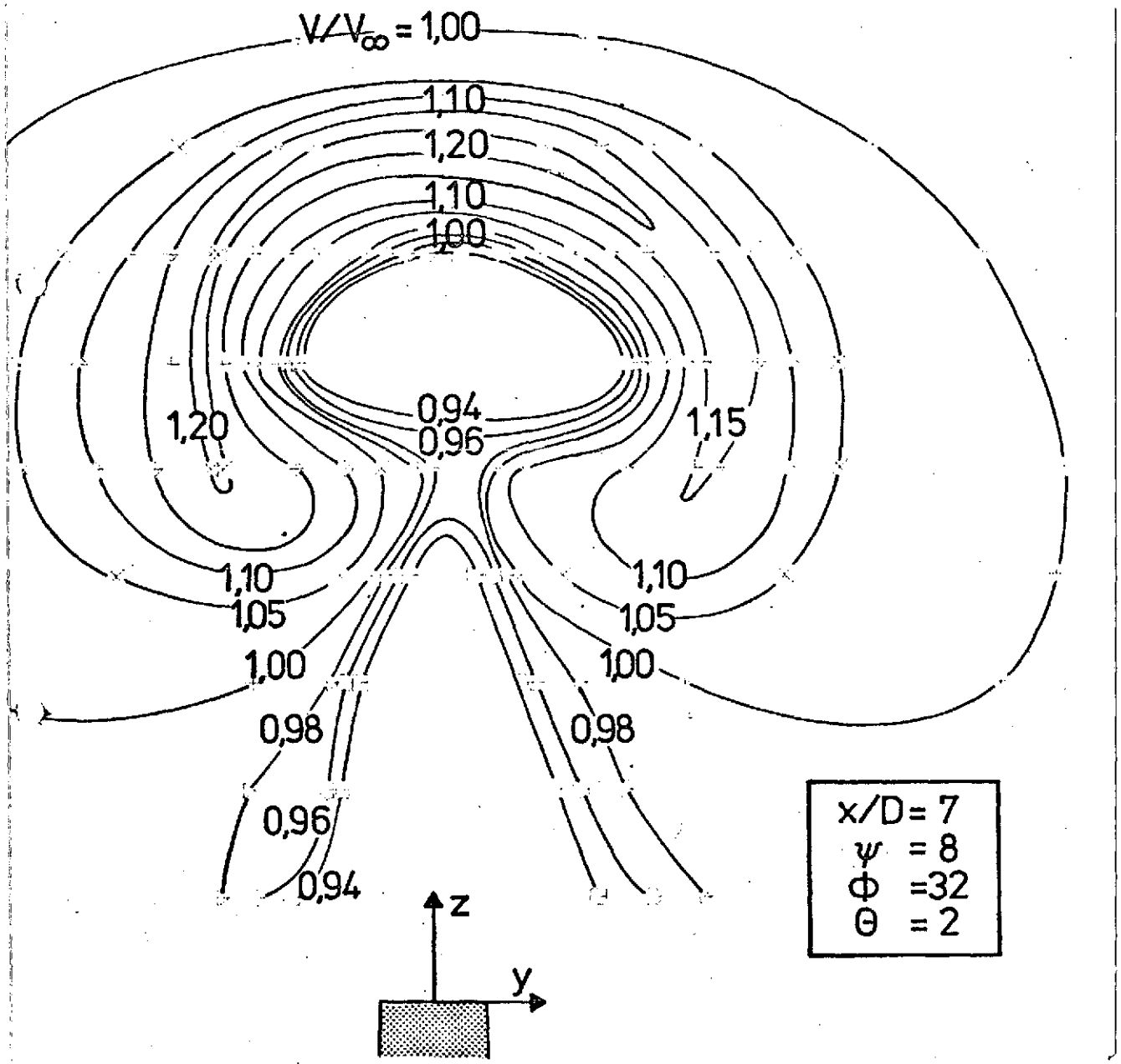

Figure 20. Velocity distribution in the transverse plane (y-z) plane) of the hot jet

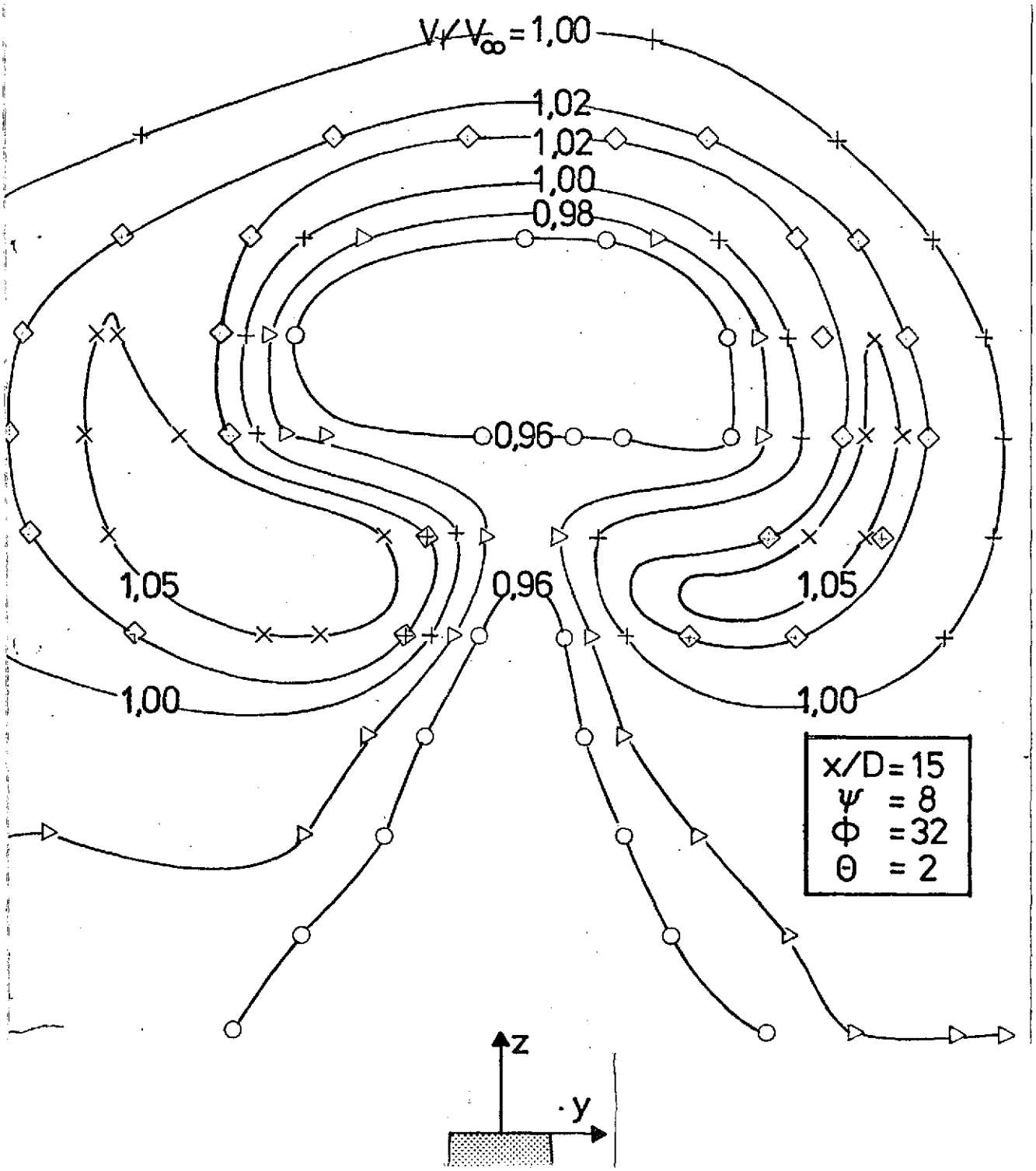

Figure 21. Velocity distribution in the transverse plane (y-z plane) of the hot jet.

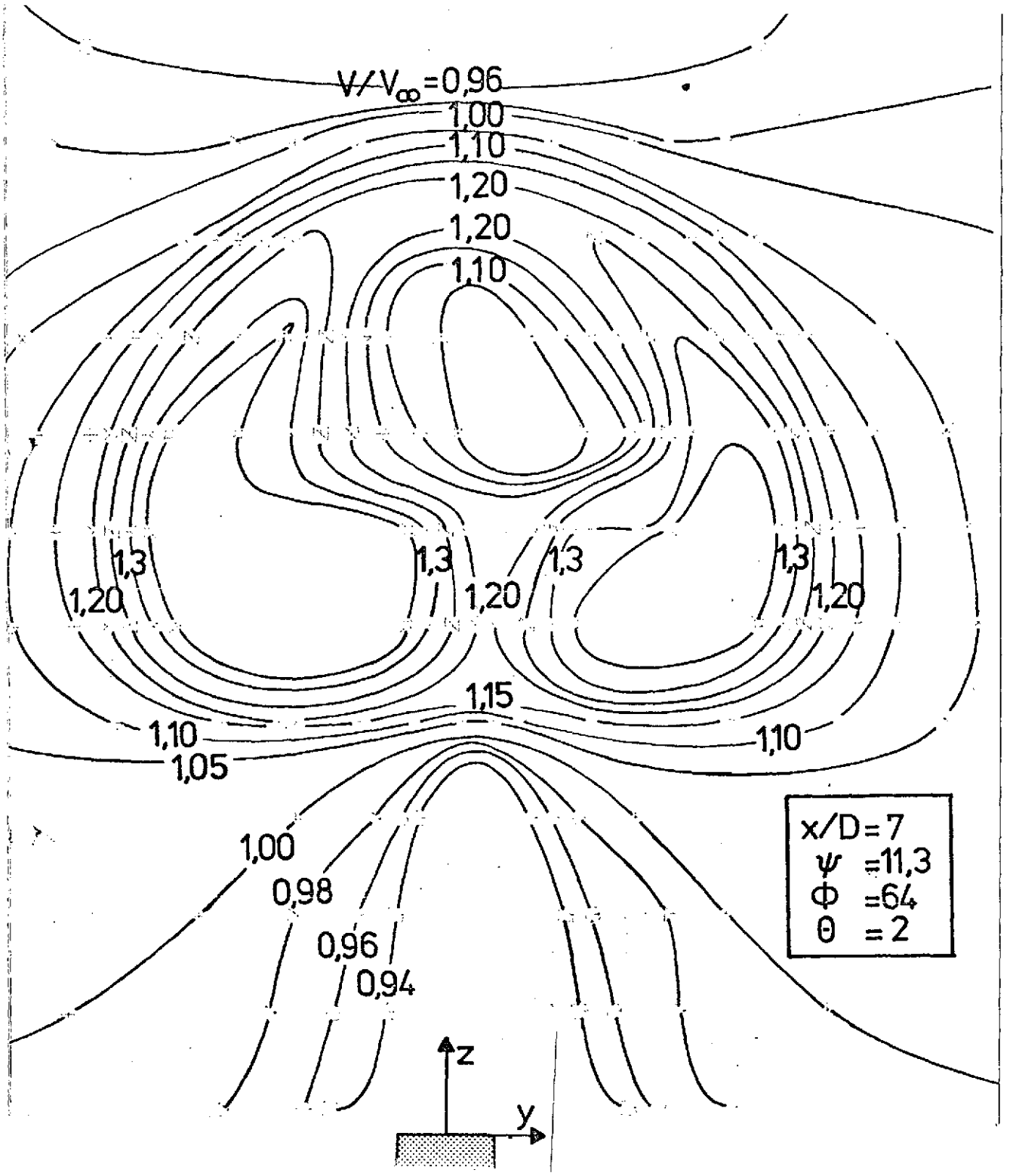

Figure 22. Velocity distribution in the transverse plane (y-z plane) of the hot jet

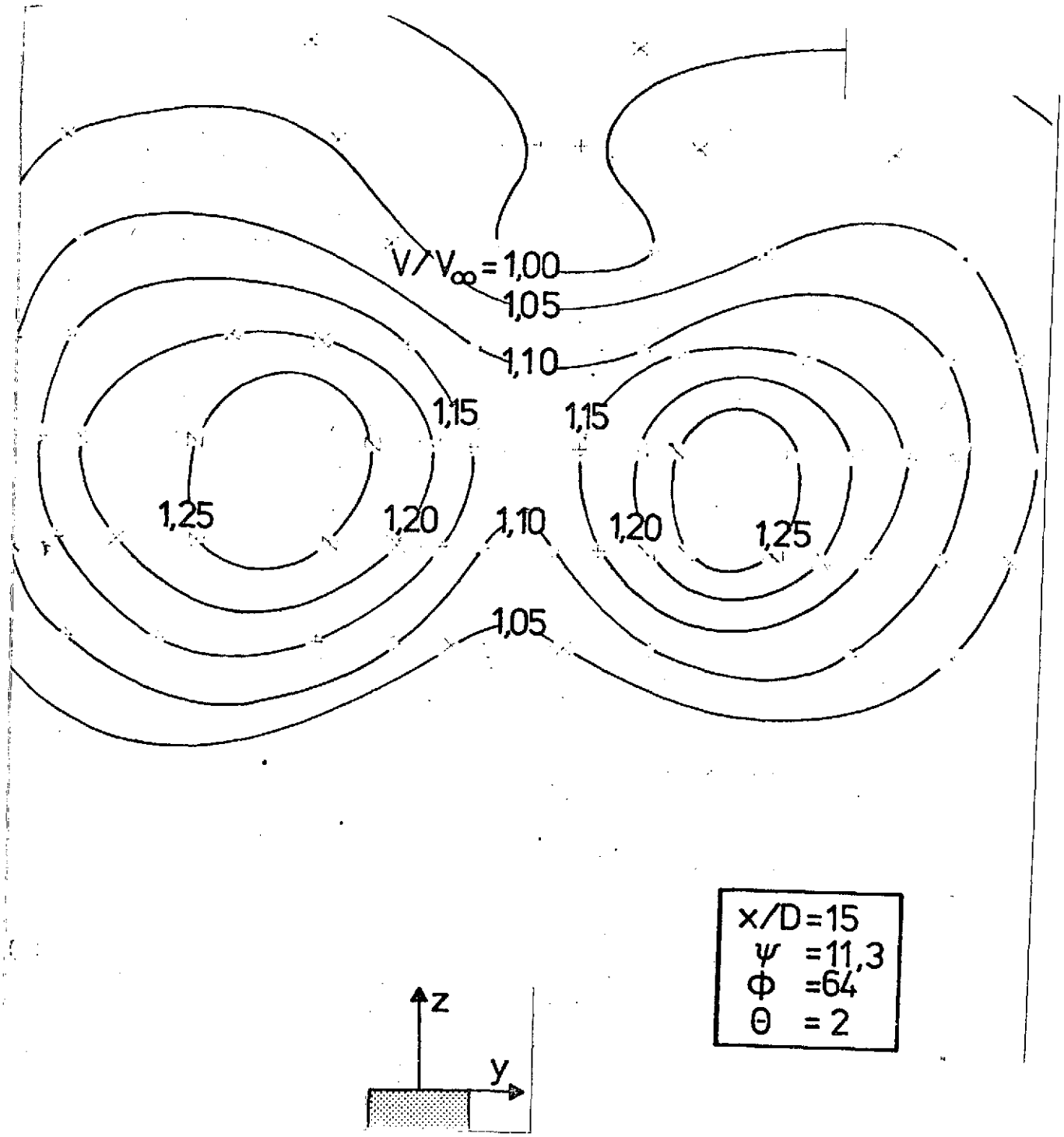

Figure 23. Velocity distribution in the transverse plane (x-y plane) of the hot jet

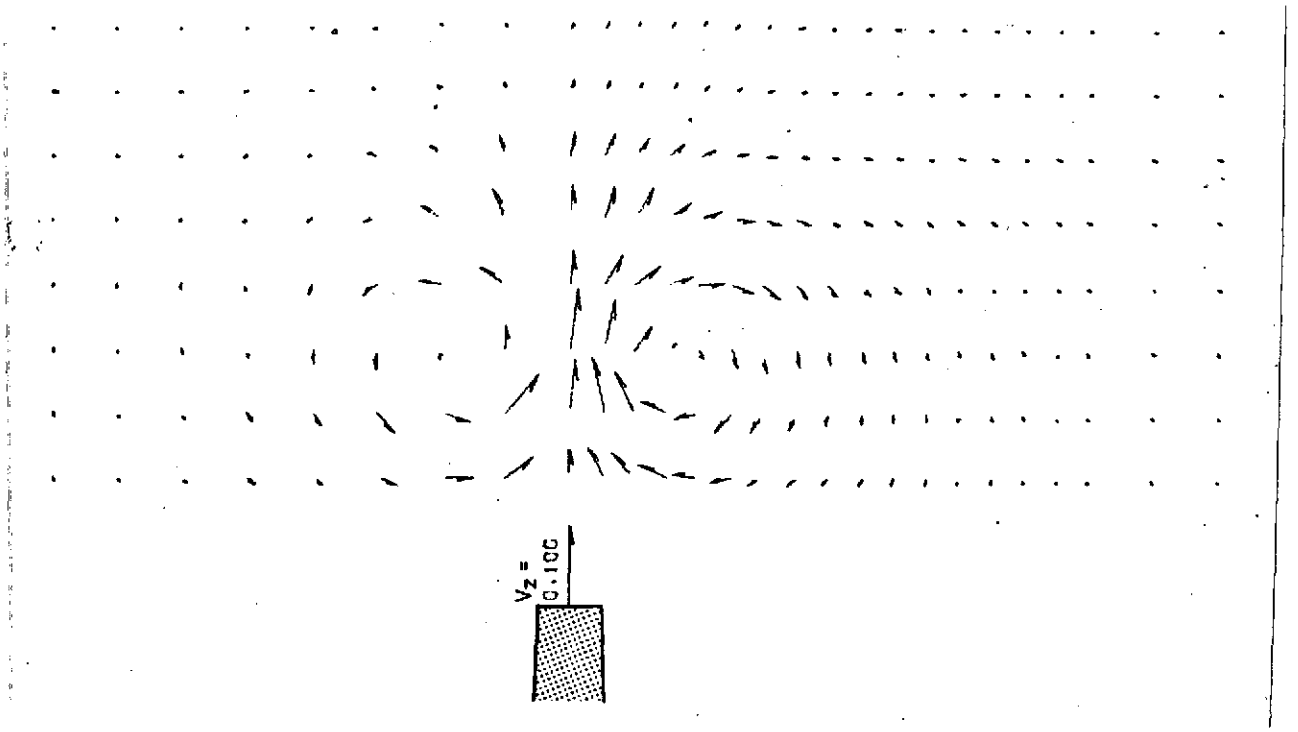

Figure 24. Representation of the velocity vectors projected on the y-z plane ($x/D = 7, \psi = 4, \Phi = 16, \Theta = 1$)

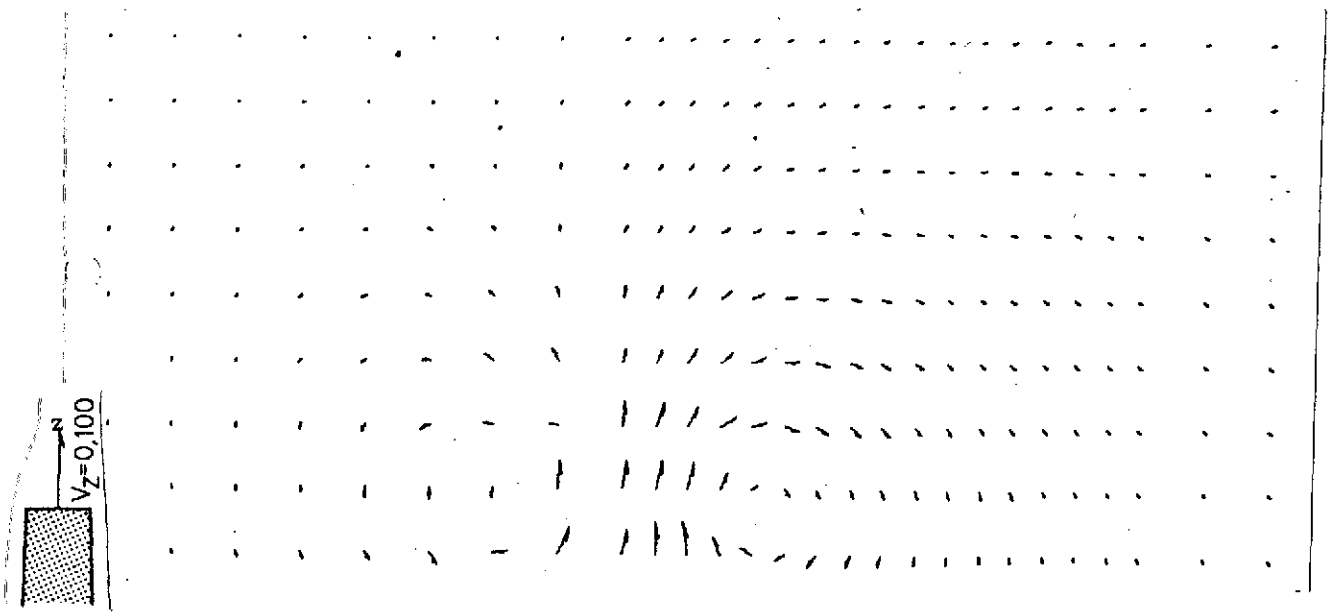

Figure 25. Representation of the velocity vectors projected on the y-z plane ($x/D = 15, \psi = 4, \Phi = 16, \Theta = 1$)

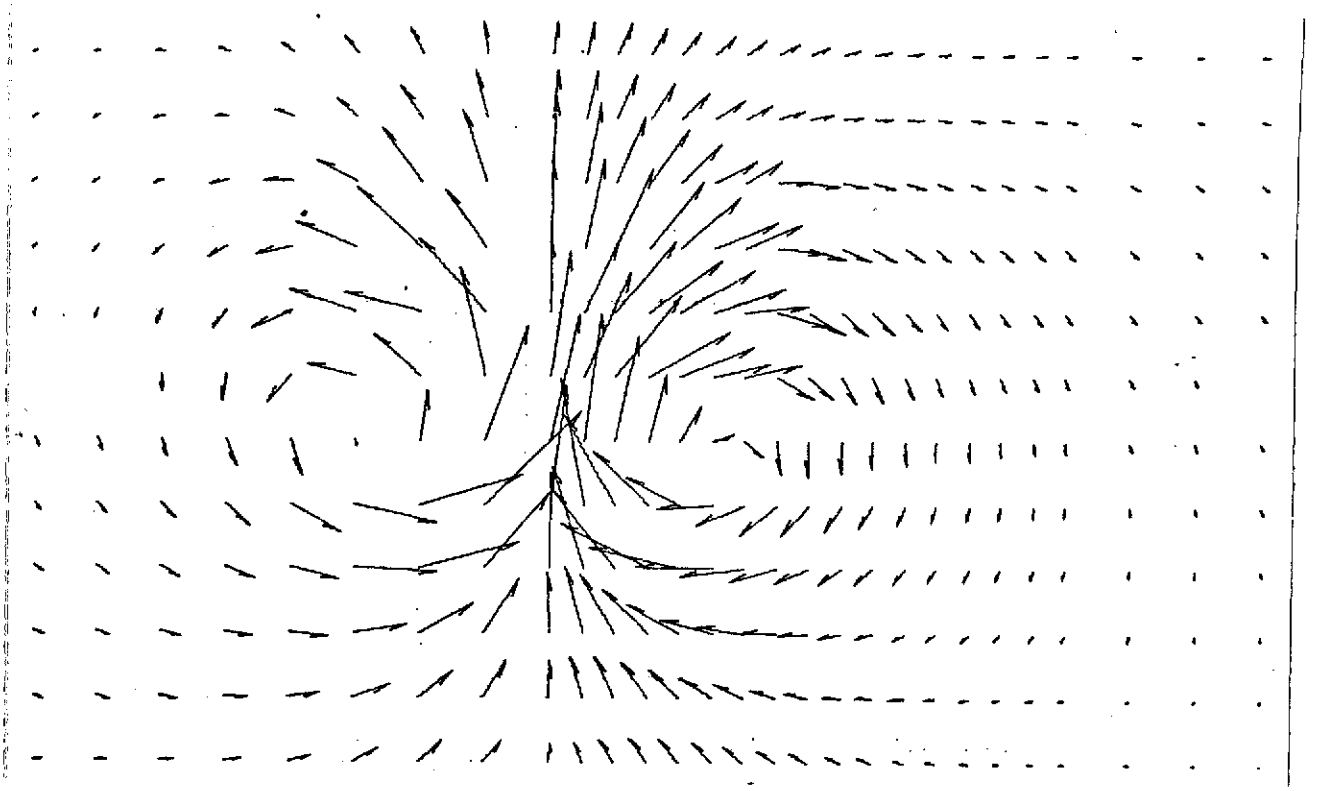

Figure 26. Representation of the velocity vectors projected on the y-z plane (x/D = 7, ψ = 8, P = 64, Θ = 1)

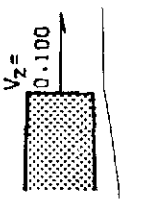

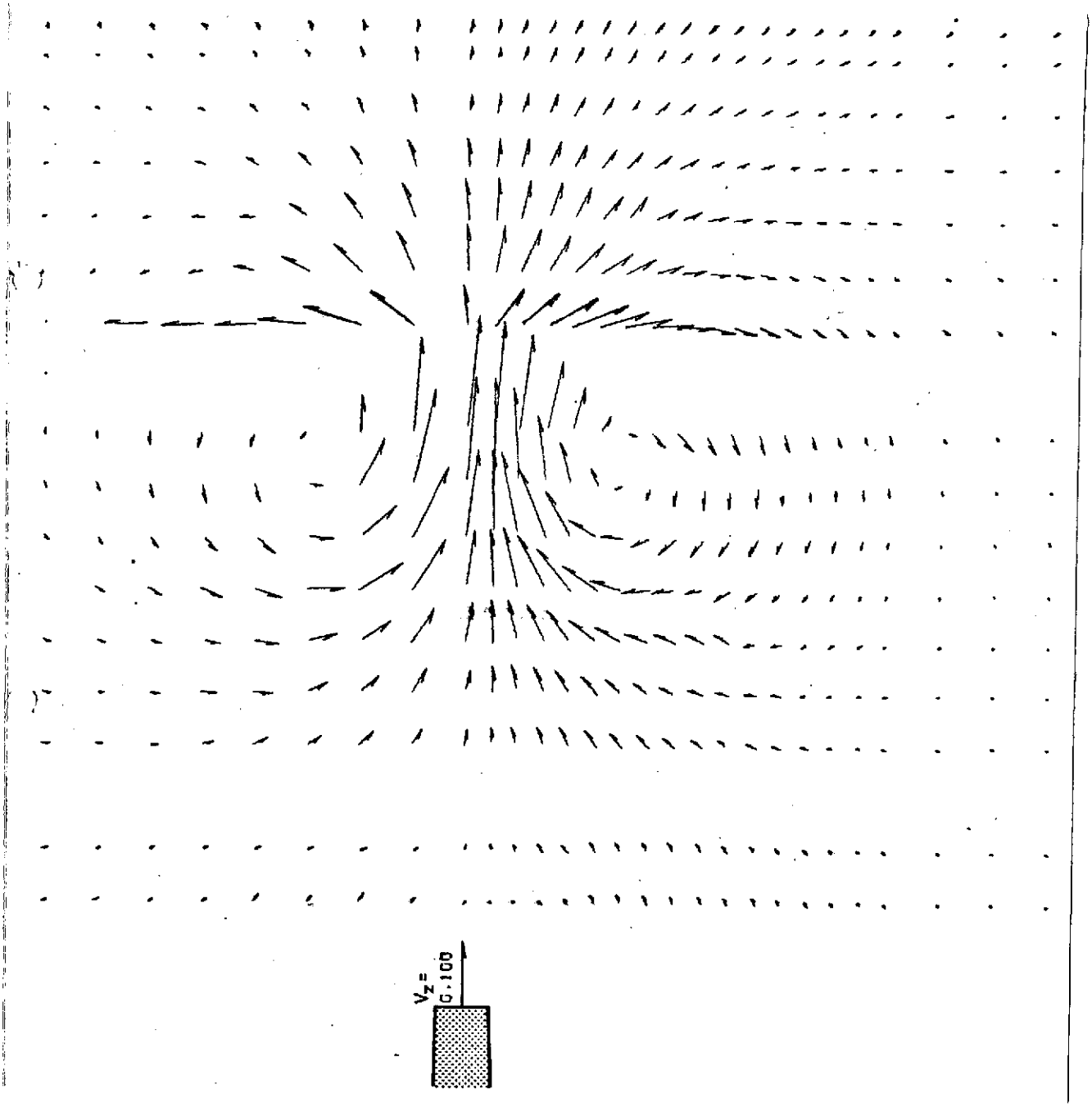

Figure 27. Representation of the velocity vectors projected on the y-z plane ($x/D = 15$, $\psi = 8$, $\phi = 64$, $\Theta = 1$)

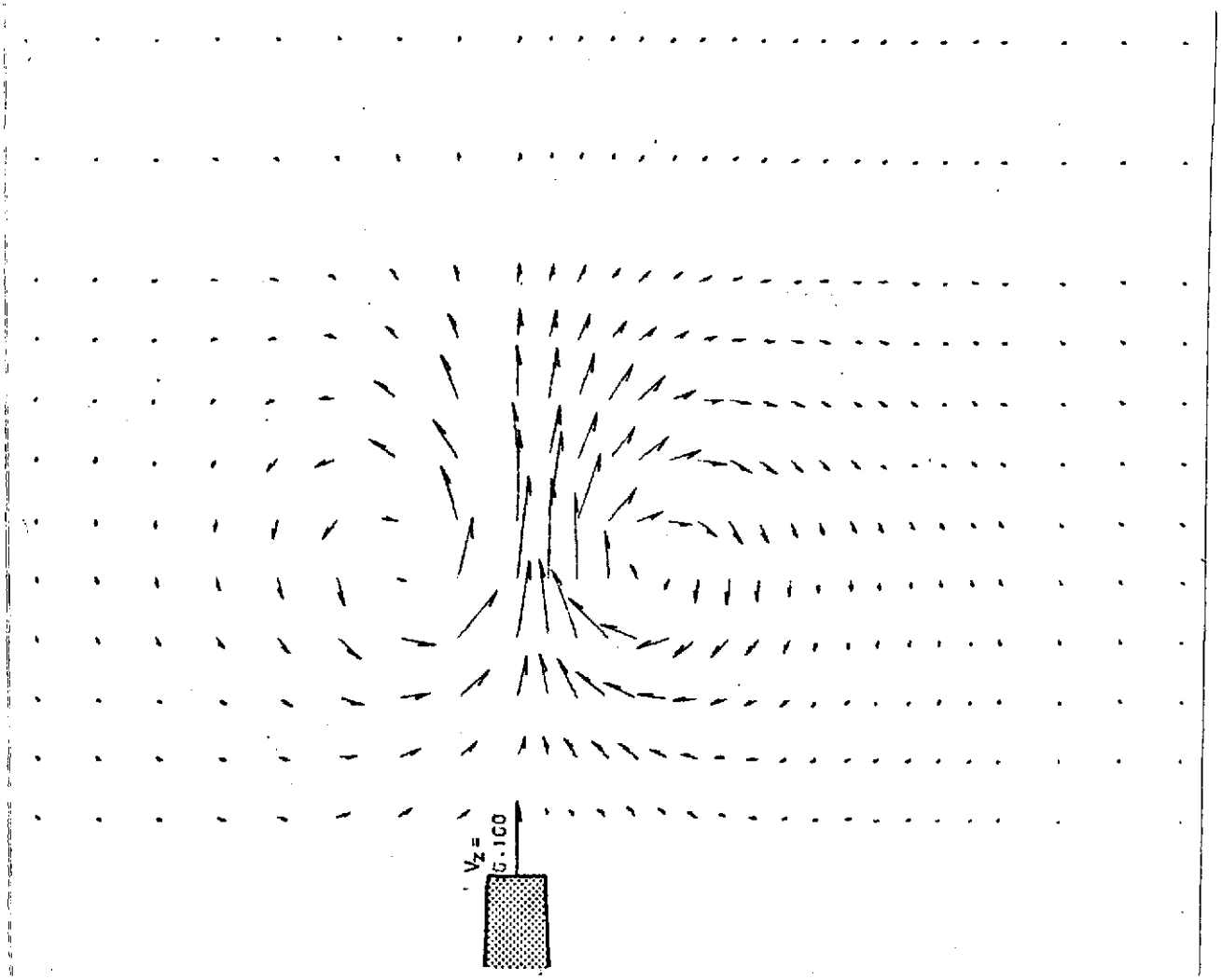

Figure 28. Representation of the velocity vectors projected on the y-z plane (x/D = 2, ψ = 8, φ = 32, Θ = 2)

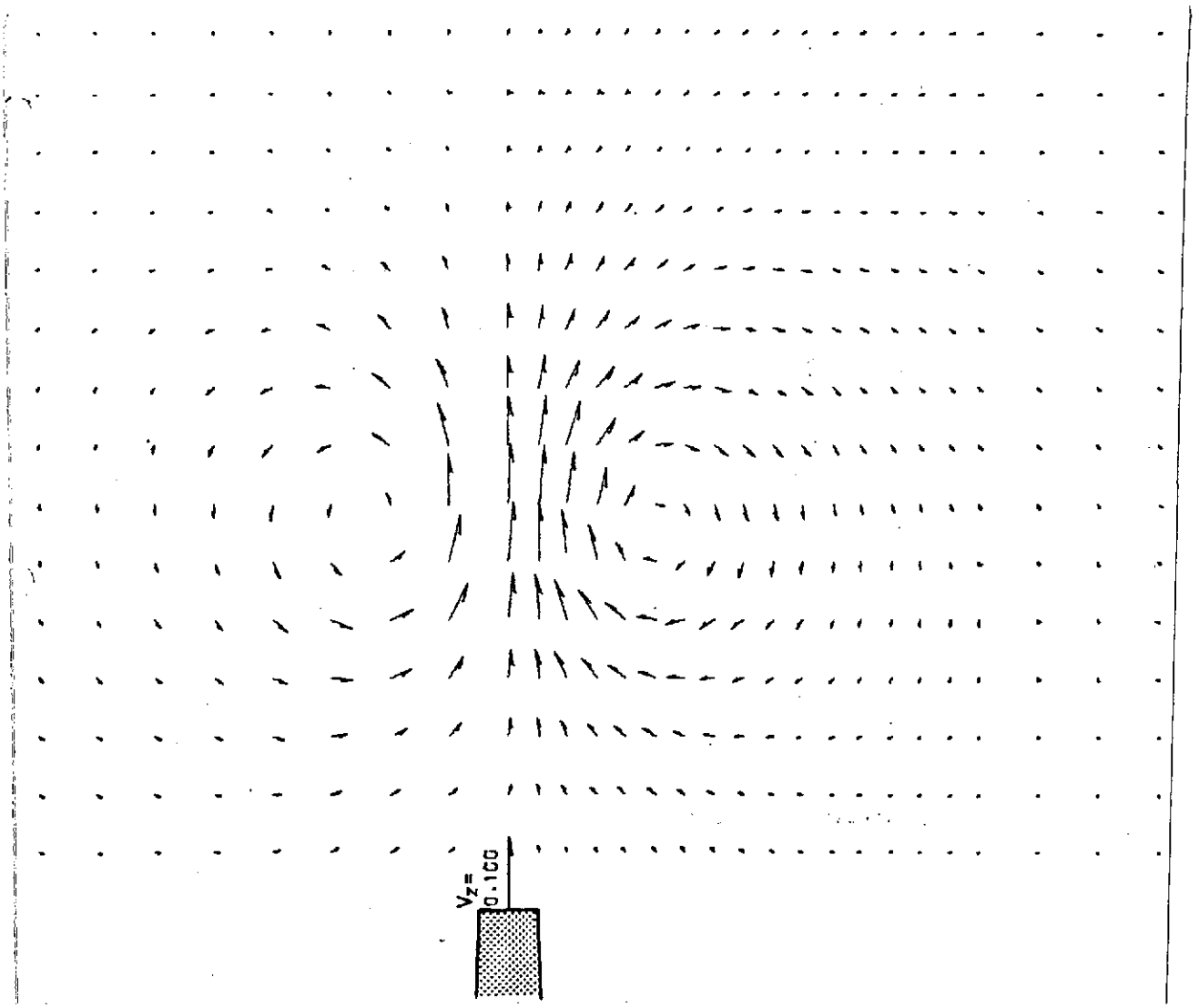

Figure 29. Representation of the velocity vectors projected on the y-z plane. ($x/D = 1.5$, $\psi = 8$, $\phi = 32$, $\theta = 2$)

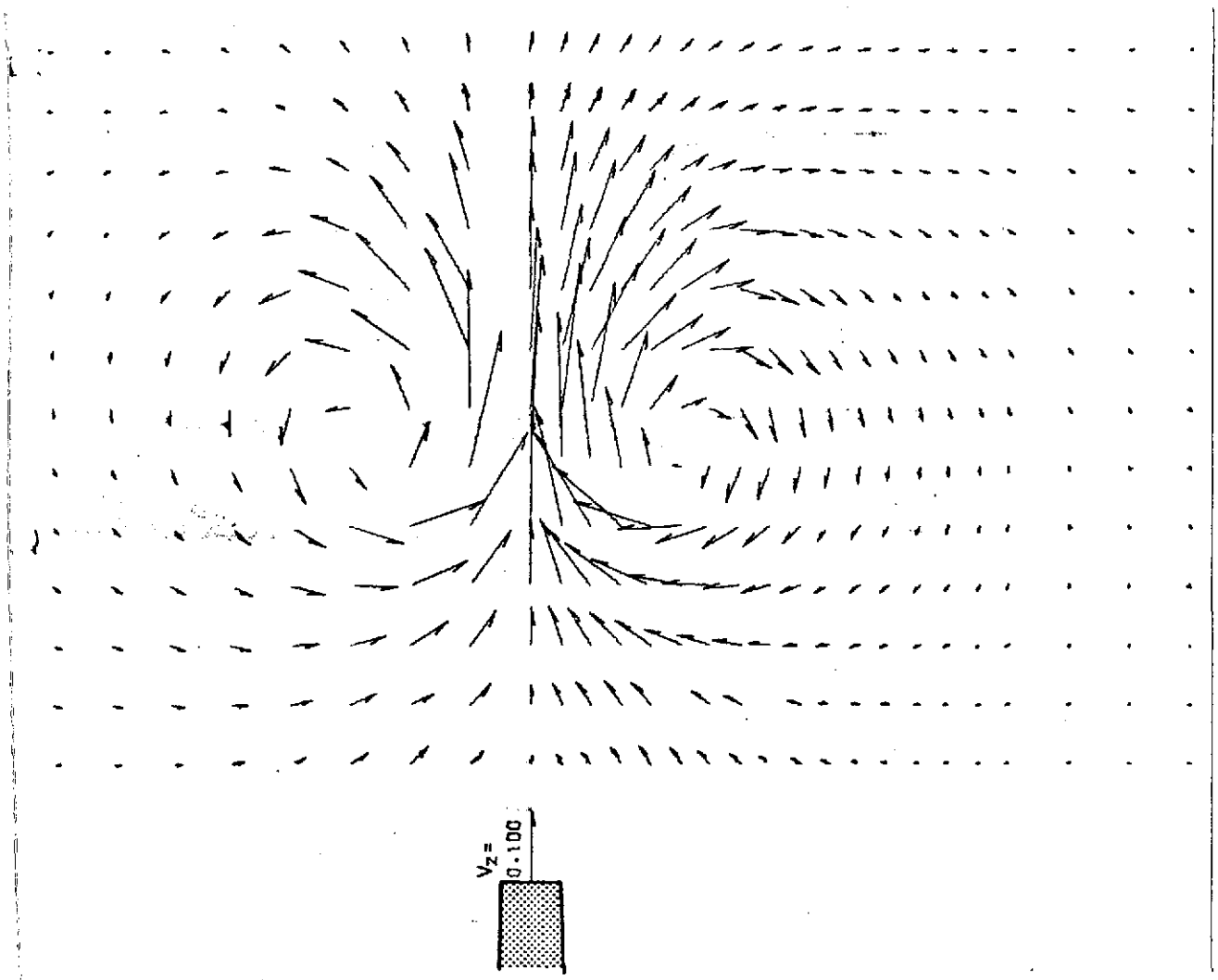

Figure 30. Representation of the velocity vectors projected on the x-y plane ($x/D = 7$, $\psi = 11,3$, $\phi = 64$, $\Theta = 2$)

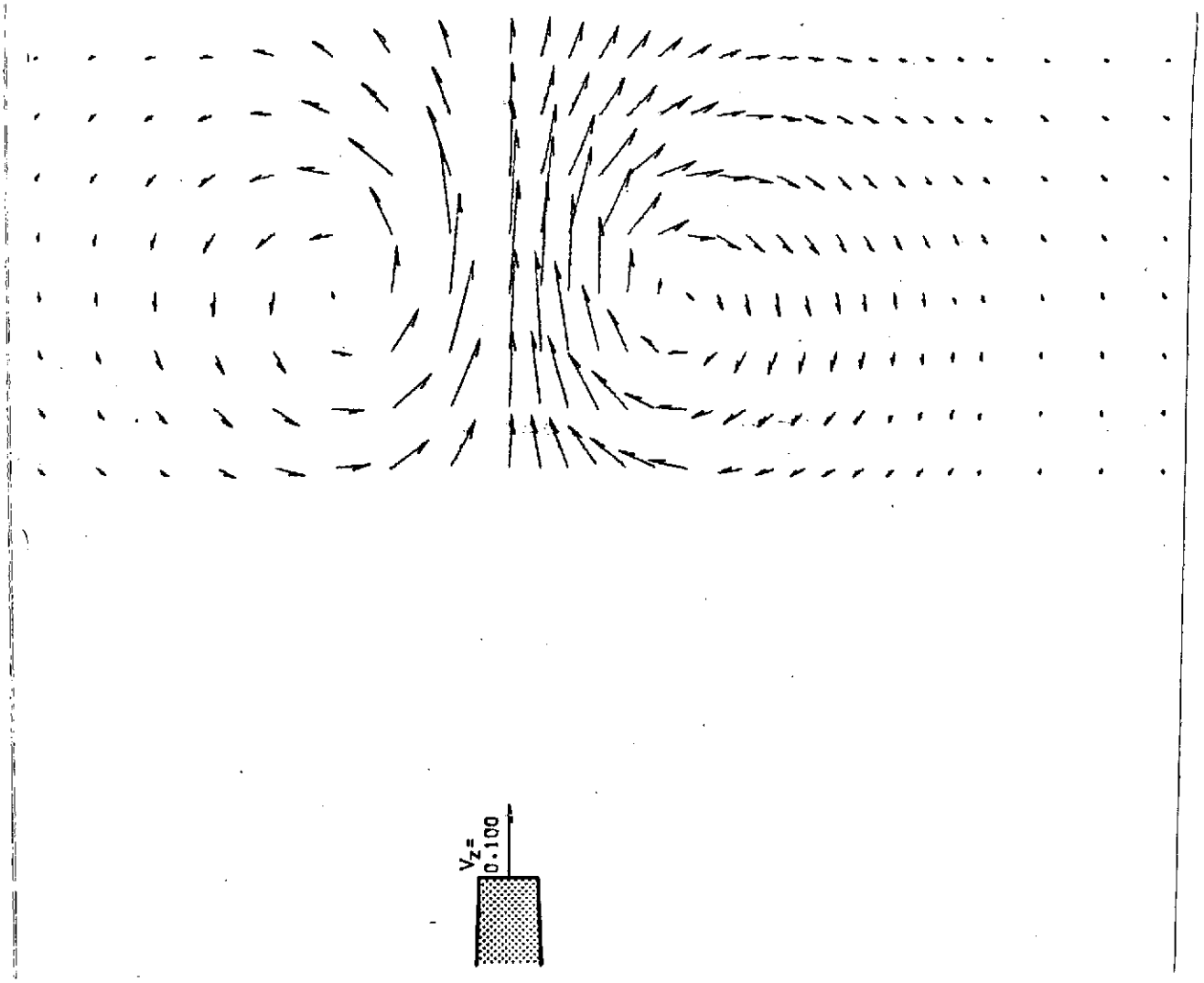

Figure 31. Representation of the velocity vectors projected on the x-y plane ($x/D = 15, \psi = 11, 3, \phi = 64, \Theta = 2$)

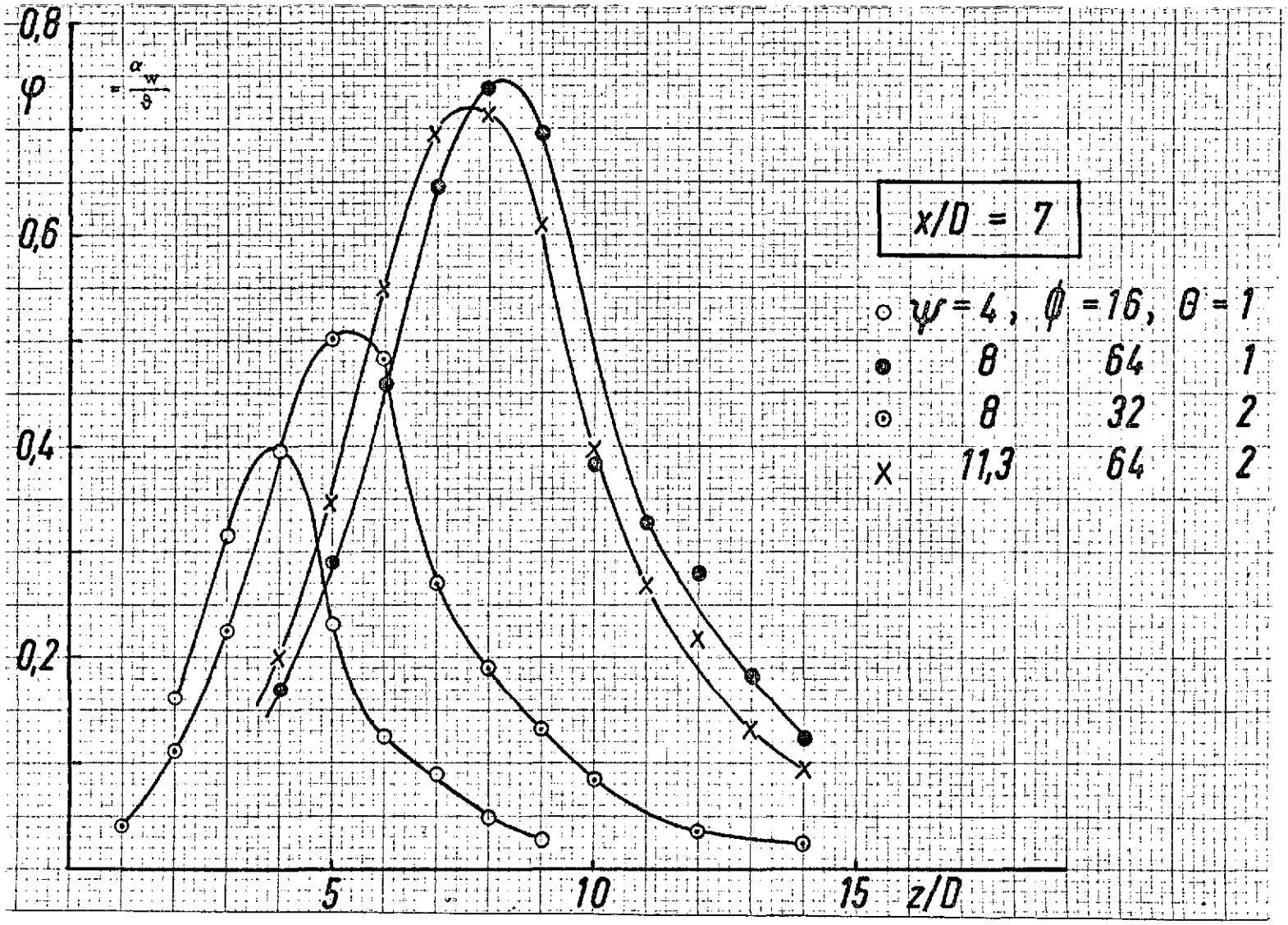

Figure 32. Local flow angle φ in the symmetry plane for various velocity ratios ψ and various momentum ratios ϕ

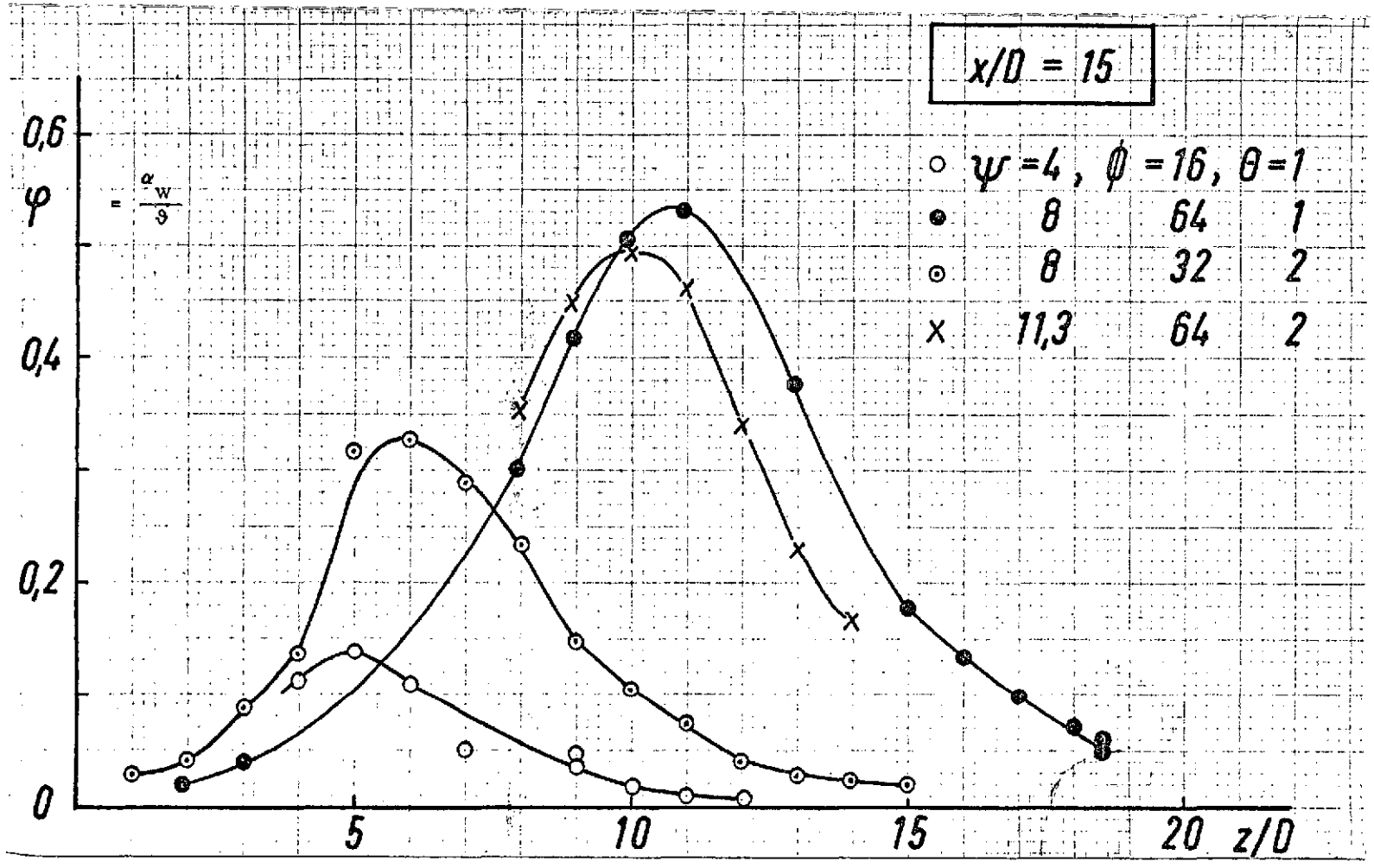

Figure 33. Local flow angle φ in the symmetry plane for various velocity ratios ψ and various momentum ratios ϕ.

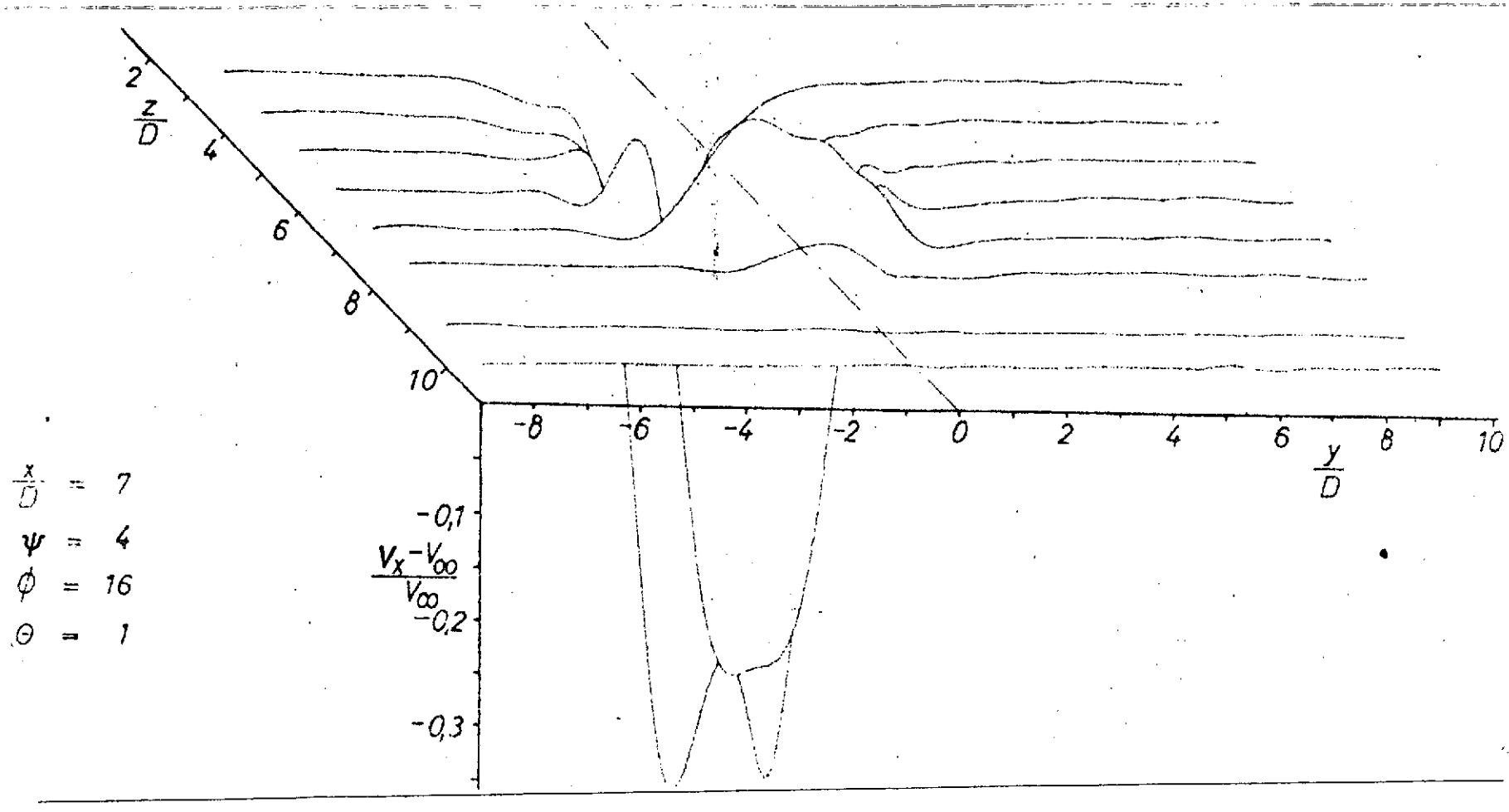

Figure 34. Three-dimensional representation of the velocity field of the cold jet.

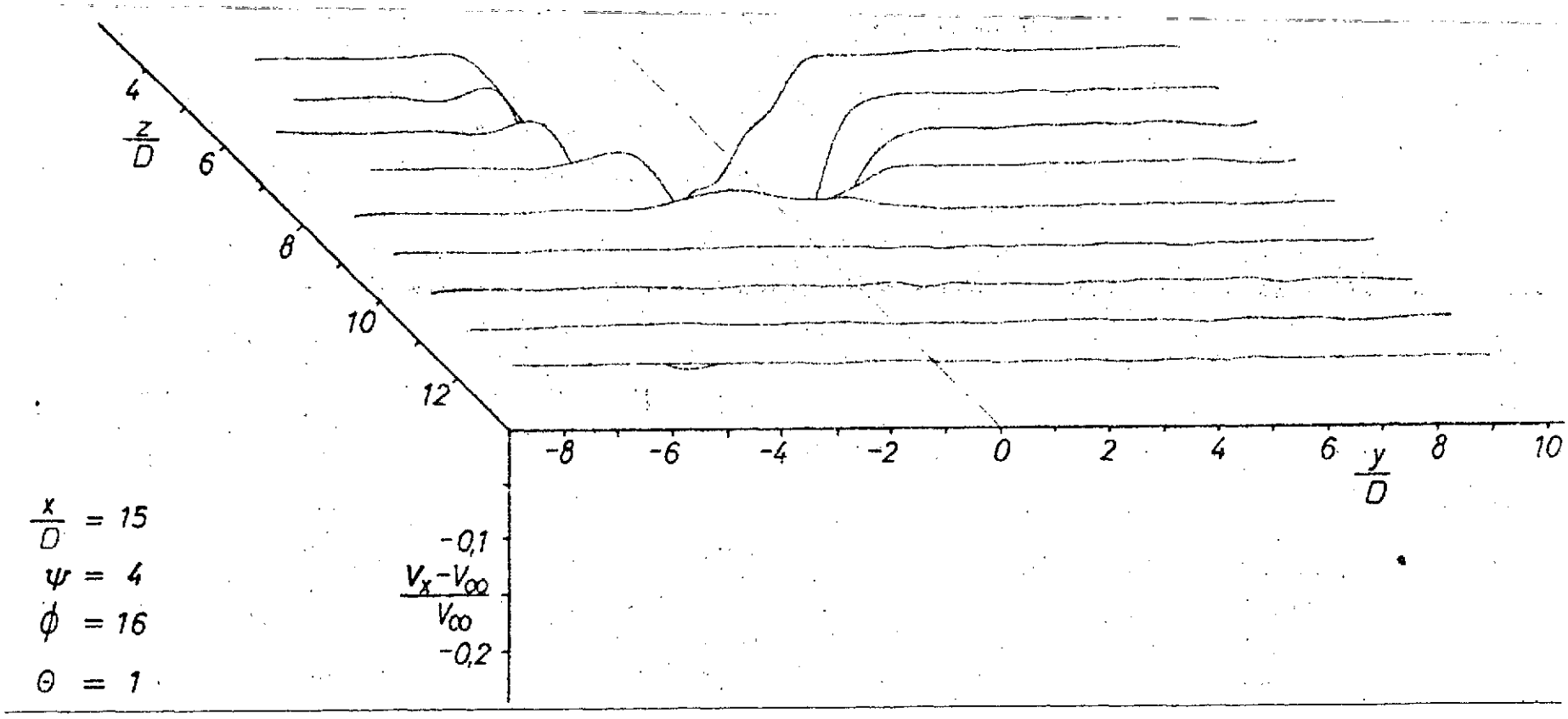

Figure 35. Three-dimensional representation of the velocity field of the cold jet.

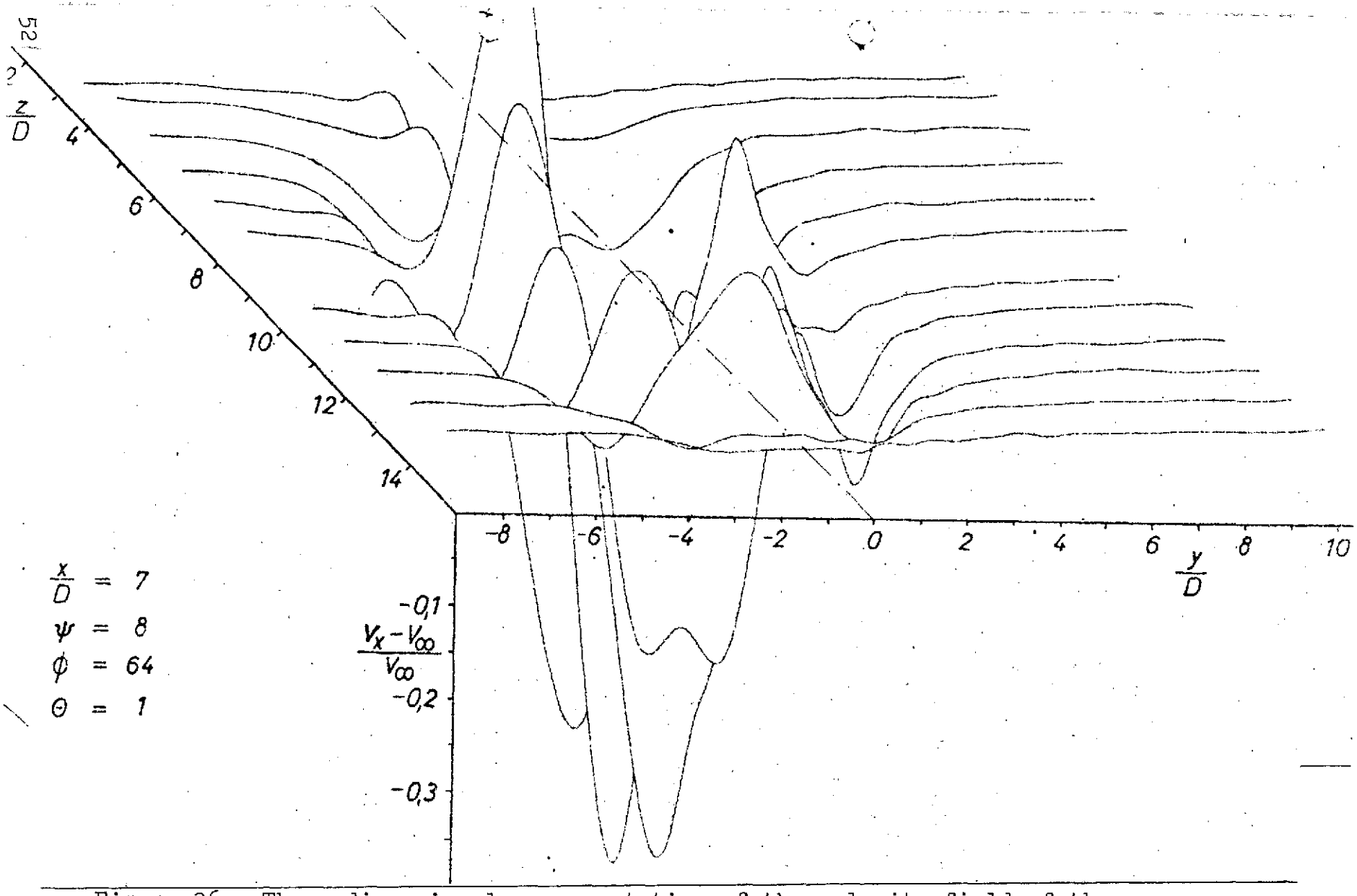

Figure 36. Three-dimensional representation of the velocity field of the cold jet

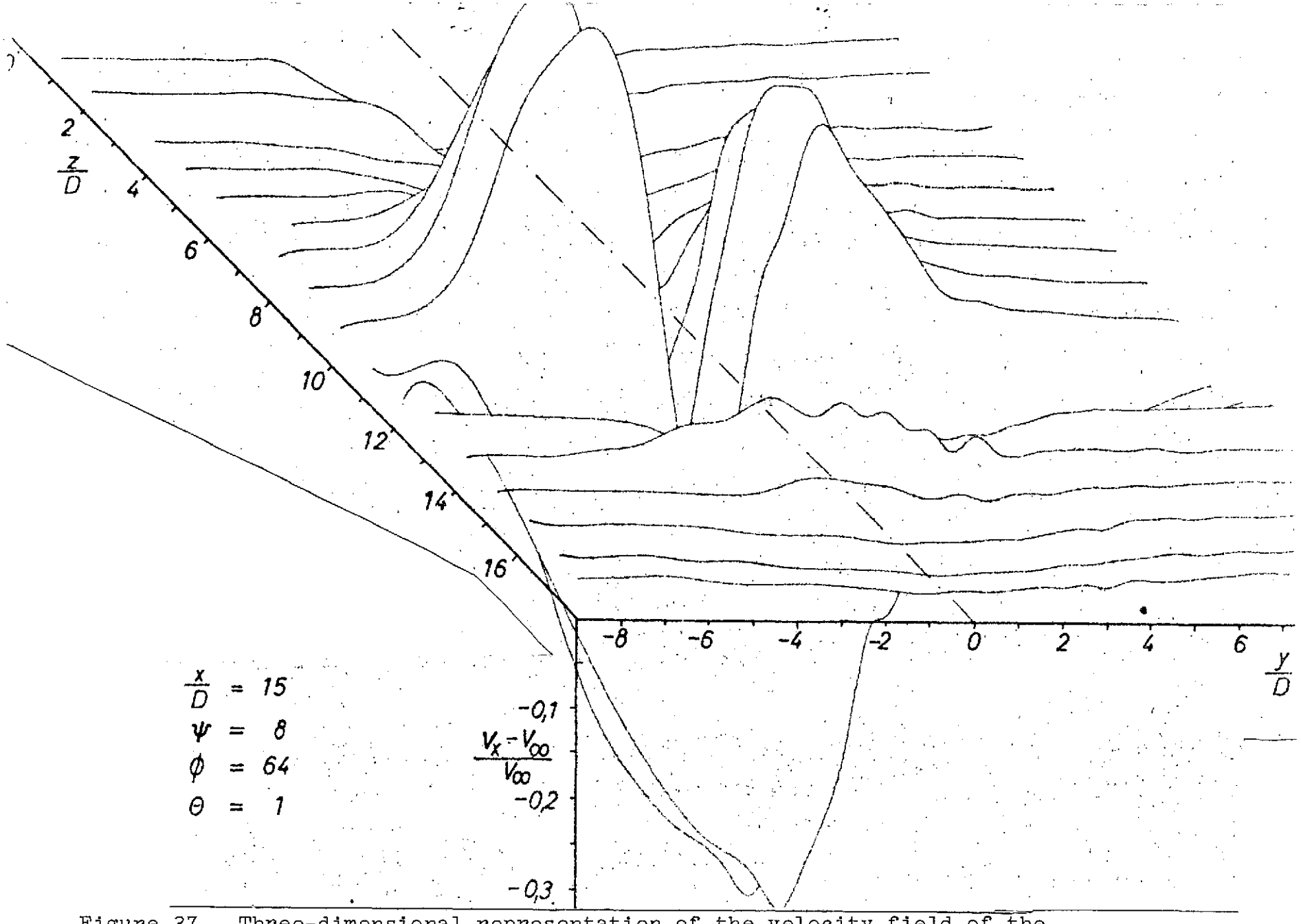

Figure 37. Three-dimensional representation of the velocity field of the cold jet.

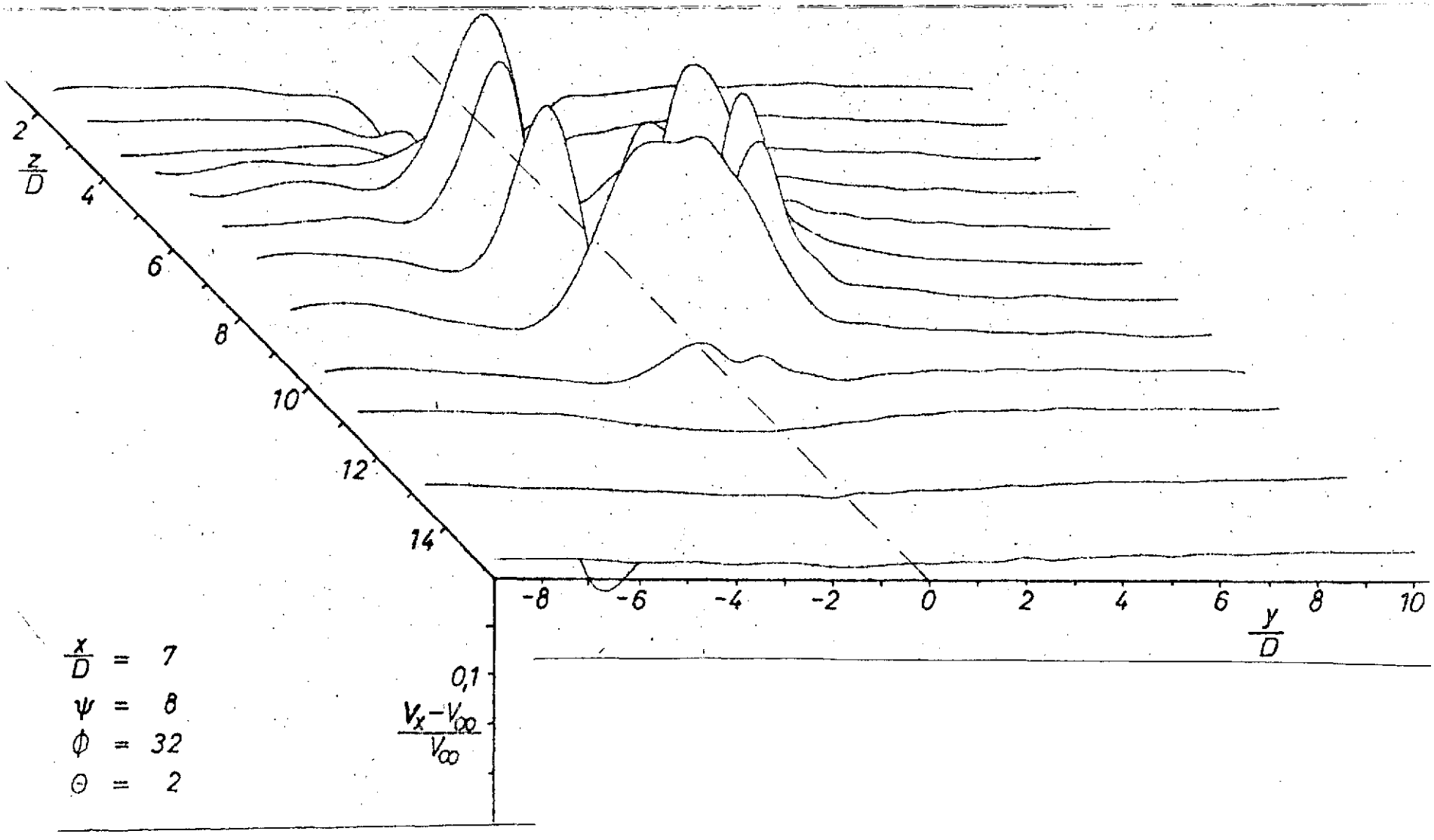

Figure 38. Three-dimensional representation of the velocity field of the hot jet.

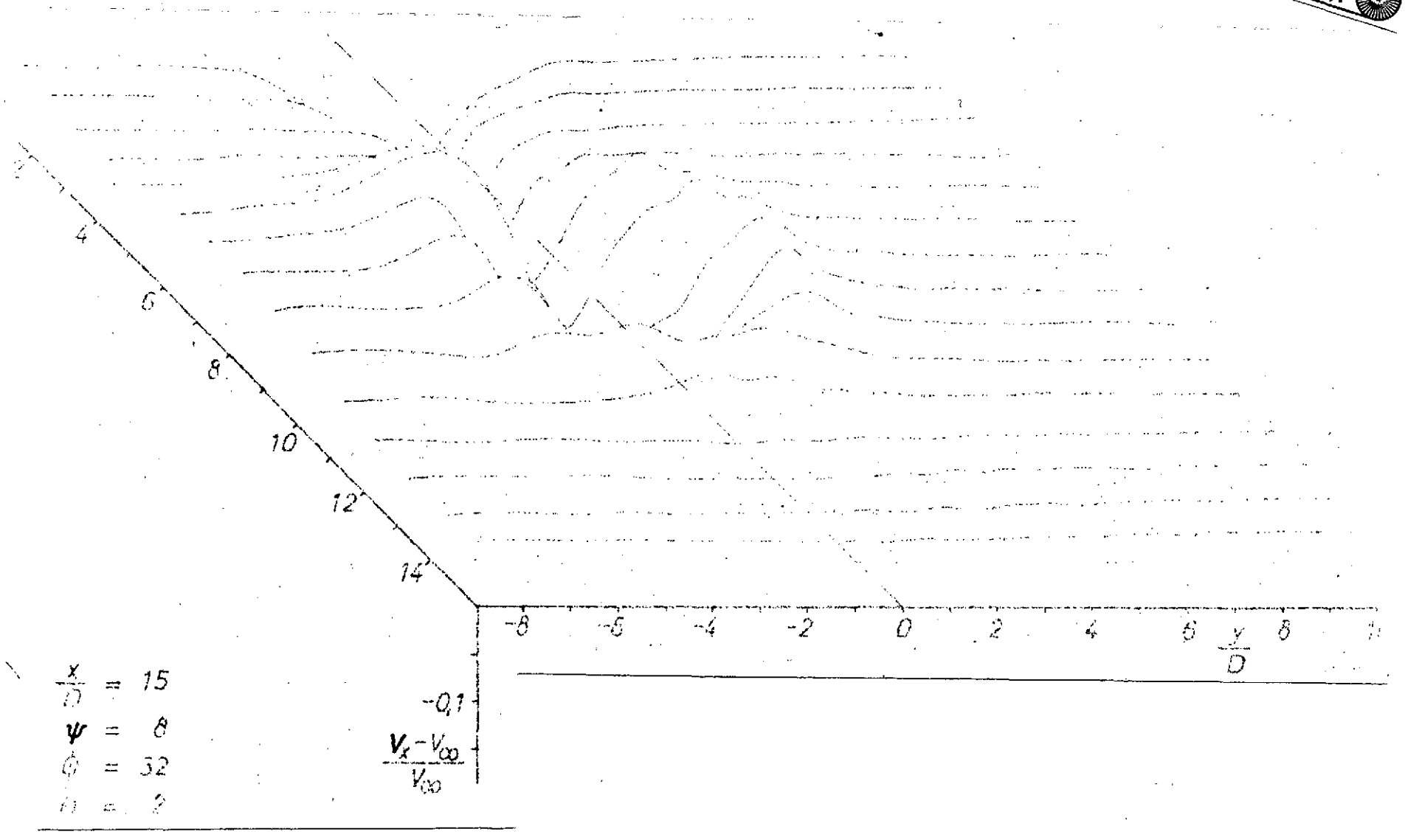

Figure 39. Three-dimensional representation of the velocity field of the hot jet

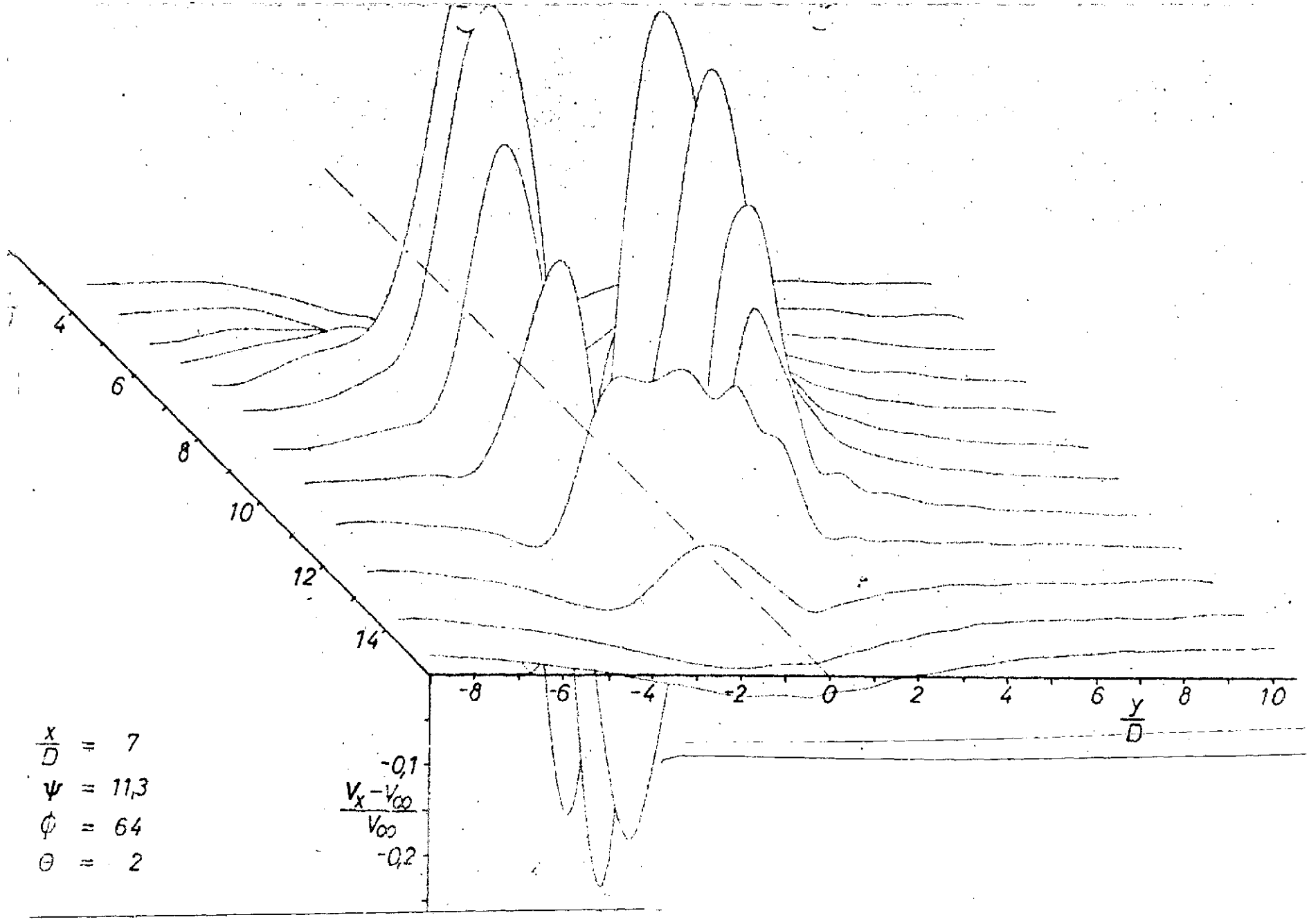

Figure 40. Three-dimensional representation of the velocity field of the hot jet

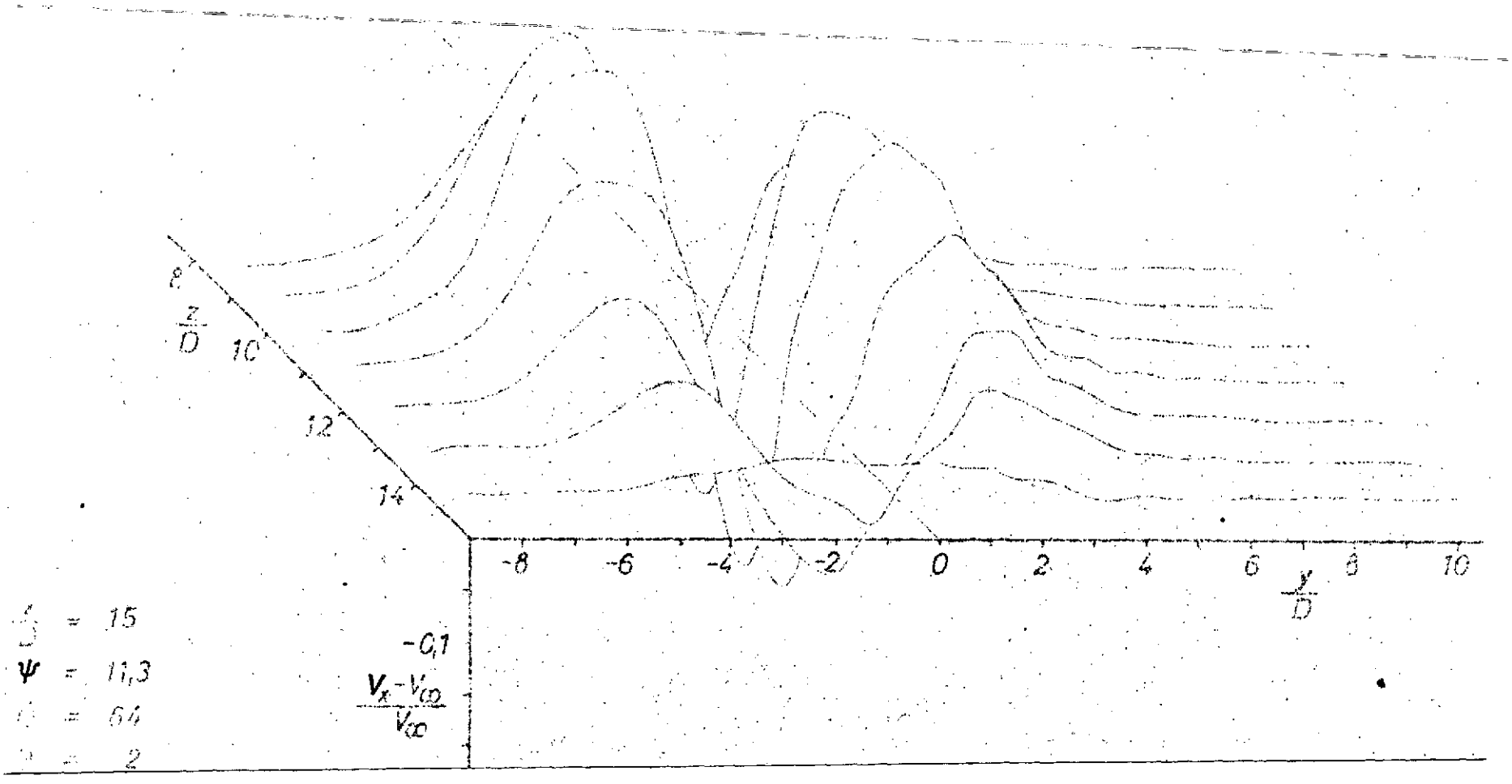

Figure 41. Three-dimensional representation of the velocity field of the hot jet

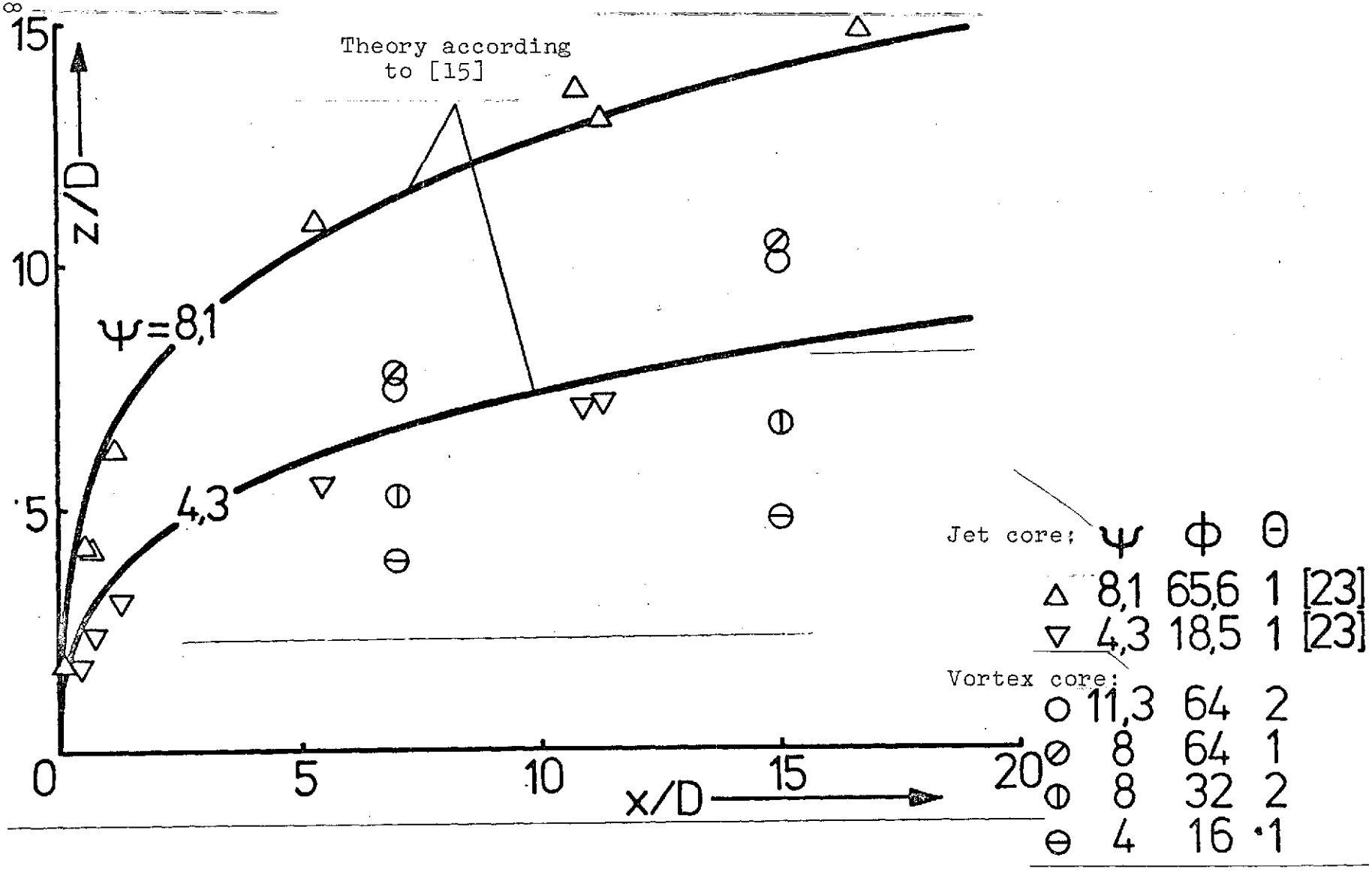

Figure 42. Comparison of the position of the vortex cores of the jet in a transverse flow with theoretical and experimental results on the variation of jet cores.